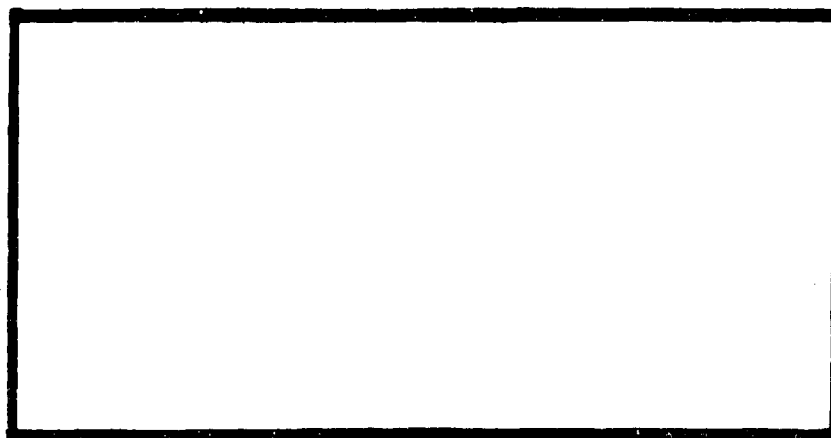


AD-A243 912



DTIC  
ELECTE  
JAN 06 1992  
S D D



This document has been approved  
for public release and sale; its  
distribution is unlimited.

92-00170



DEPARTMENT OF THE AIR FORCE  
AIR UNIVERSITY  
**AIR FORCE INSTITUTE OF TECHNOLOGY**

Wright-Patterson Air Force Base, Ohio

92 1 2 143

AFIT/GAE/ENY/91D-4



AN EXPERIMENTAL STUDY OF A STING-  
MOUNTED CIRCULATION CONTROL WING

THESIS

Steven J. Lacher, Captain, USAF

AFIT/GAE/ENY/91D-4

Approved for public release; distribution unlimited

AFIT/GAE/ENY/91D-4

AN EXPERIMENTAL STUDY OF A  
STING-MOUNTED  
CIRCULATION CONTROL WING

THESIS

Presented to the Faculty of the School of Engineering  
of the Air Force Institute of Technology  
Air University  
In Partial Fulfillment of the  
Requirements for the Degree of  
Master of Science in Aeronautical Engineering



Steven J. Lacher, B.S.

Captain, USAF

December 1991

Accession For	
NTIS CRA&I	<input checked="" type="checkbox"/>
DTIC TAB	<input type="checkbox"/>
Unannounced	<input type="checkbox"/>
Justification	
By	
Distribution/	
Availability Codes	
Dist	Avail and/or Special
A-1	

Approved for public release; distribution unlimited

### Acknowledgements

I would like to thank the people without whose help, I could not have completed this thesis. Dr. Milton Franke, my advisor, got me interested in this research and forced me to keep going when the pitfalls of experimental research threatened to overwhelm the ambition of the researcher. Mr. Dan Rioux provided excellent technical support with instrumentation and wind tunnel operation. Mr. Jay Anderson helped procure equipment absolutely necessary to perform pulsed blowing tests. Mr. Steve DeCook provided very timely help in understanding the force balance and tunnel data acquisition system when nothing seemed to make sense.

## Table of Contents

Acknowledgements .....	ii
List of Symbols .....	vii
Abstract .....	xii
I. Introduction .....	1
Background .....	1
Previous Research .....	6
Present Study .....	7
II. Test Item Description and Instrumentation .....	8
Wing Model .....	8
Blowing Air Supply System .....	14
Pulser Valve .....	16
AFIT 5-ft Wind Tunnel .....	18
Data Acquisition System and Force Balance ....	20
III. Experimental Procedure .....	24
Calibration .....	24
Theory .....	26
Model Checkout .....	28
Preliminary Testing .....	29
Primary Testing .....	45
IV. Data Reduction .....	47
Momentum Coefficient .....	47
Wind Tunnel Corrections .....	47
Lift Coefficient .....	49
Drag Coefficient .....	53
Equivalent Drag .....	55
Pitching Moment About the Leading Edge .....	56
Pressure Coefficient .....	59
Pulsed Blowing .....	60
V. Results and Discussion .....	62
Preliminary Testing .....	62
Primary Testing .....	63
VI. Conclusions .....	88
VII. Recommendations .....	89
References .....	91
Appendix 1 Reduced Data .....	95
Appendix 2 Data Accuracy .....	119

Force Balance and Wind Tunnel Data .....	119
Surface Pressure Data .....	119
Atmospheric Data .....	119
Secondary Air Data .....	119
Overall Accuracy .....	120
Vita .....	121

## List of Figures

Figure 1.	Wing Cross-section .....	9
Figure 2.	Wing Planform .....	11
Figure 3.	Blowing Slot Detail .....	12
Figure 4.	Secondary Air Supply .....	16
Figure 5.	Pulser Valve .....	18
Figure 6.	Data Acquisition System Hardware .....	24
Figure 7.	Initial Jet Velocity Profile .....	31
Figure 8.	Jet Velocity Profile After Adjustment .....	32
Figure 9.	Photos of Wing in Wind Tunnel .....	37
Figure 10.	Photo of Wing and Pulser .....	38
Figure 11.	Wing Basic Lift Coefficients .....	39
Figure 12.	Wing Basic Drag Coefficients .....	40
Figure 13.	Wing Basic Moment Coefficients .....	41
Figure 14.	Axial Force Due to Jet Thrust .....	42
Figure 15.	Normal Force Due to Jet Thrust .....	43
Figure 16.	Lift Coeff/Momentum Coeff. vs Momentum Coeff. ....	61
Figure 17.	Lift Coefficient vs Momentum Coefficient .....	65
Figure 18.	Extrapolated Lift Coeff. vs Momentum Coeff. ....	66
Figure 19.	Lift Coeff. vs Momentum Coeff. - Jet Tripped .....	68
Figure 20.	Drag Coeff vs Momentum Coeff .....	69
Figure 21.	Drag Coeff vs Momentum Coeff - Jet Tripped .....	70
Figure 22.	Moment Coefficient vs Momentum Coefficient .....	72
Figure 23.	Moment Coeff vs Momentum Coeff - Jet Tripped .....	73
Figure 24.	Pressure Coefficient Alpha = 0; Cmu = 0 .....	75
Figure 25.	Pressure Coefficient Alpha = +1; Cmu = 0.1816 .....	76
Figure 26.	Pressure Coefficient Alpha = +18; Cmu = 0.1877 .....	77
Figure 27.	Pressure Coefficient Alpha = +18; Cmu = 0.1820 .....	78
Figure 28.	Pressure Coefficient Alpha = +18; Cmu = 0.1820 .....	79
Figure 29.	Lift to Equivalent Drag Ratio .....	82
Figure 30.	CL/Cmu vs Frequency - Low Cmu .....	85
Figure 31.	CL/Cmu vs Frequency - Med Cmu .....	86
Figure 32.	CL/Cmu vs Frequency - High Cmu .....	87

## List of Tables

Table 1.	Static Pressure Port Locations .....	14
Table 2.	Typical Lift Corrections .....	52
Table 3.	Typical Drag Corrections .....	54
Table 4.	Typical Moment Coefficient Corrections .....	58
Table 5.	Comparison of Measured and Calculated Lift Coeff. ....	80



### List of Symbols

		Units
A	constant coefficient	
AR	wing aspect ratio or Venturi area ratio	
AX	force balance axial force	lb <sub>f</sub>
c	wing chord	ft
C <sub>D</sub>	wing drag coefficient	
C <sub>De</sub>	wing equivalent drag coefficient	
C <sub>L</sub>	wing lift coefficient	
C <sub>l</sub>	section lift coefficient	
C <sub>L0</sub>	theoretical wing lift coefficient without vortex sheet deflection	
C <sub>F</sub>	pressure coefficient	
C <sub>M</sub>	moment coefficient	
C <sub>μ</sub>	momentum coefficient	
C <sub>mu</sub>	momentum coefficient	
C <sub>0</sub>	offset coefficient	lb <sub>f</sub> /in <sup>2</sup>
C <sub>1</sub>	sensitivity coefficient	lb <sub>f</sub> /in <sup>2</sup> -volt

$C_2$	nonlinearity coefficient	$\text{lb}_f/\text{in}^2\text{-volt}^2$
D	wing drag	$\text{lb}_f$
$D_e$	wing equivalent drag	$\text{lb}_f$
h	blowing slot height	in
k	constant exponent	
L	wing lift	$\text{lb}_f$
LE	wing leading edge	
$\dot{m}$	mass flow rate	slugs/sec
M	Mach number	
N1	force balance normal force on element 1	$\text{lb}_f$
N2	force balance normal force on element 2	$\text{lb}_f$
P	absolute pressure	psf
PR	Venturi pressure ratio	
q	dynamic pressure	psf
r	radius of Coanda surface	in
	or	
	perpendicular distance from vortex filament	ft

R	universal gas constant	$= 1716 \frac{ft-lb_f}{slug-deg R}$
Re	Reynolds number	
RM	rolling moment on force balance	ft-lb <sub>f</sub>
S	wing planform area	ft <sup>2</sup>
$d\bar{S}$	differential vector arc length	
T	Temperature	deg R
V	velocity	ft/sec
$\bar{V}$	vector velocity parallel to surface	ft/sec
v	specific volume	ft <sup>3</sup> /slug
$\dot{W}$	weight flow rate	lb <sub>f</sub> /sec
w	induced downwash velocity	ft/sec
x	chordwise position	ft
X	general variable	
y	spanwise position	ft
Y	general variable	
Y1	force balance lateral force on element 1	lb <sub>f</sub>
Y2	force balance lateral force on element 2	lb <sub>f</sub>

$z$	airfoil dimension normal to the chord	ft
$\alpha$	angle of attack	deg
$\gamma$	circulation per unit length	ft/sec
	or	
	ratio of specific heats of air	= 1.4
$\Gamma$	circulation	ft <sup>2</sup> /sec
$\mu$	dynamic viscosity of air	= $\frac{0.0373 \text{ slugs}}{\text{ft} - \text{sec}}$

### Subscripts

$\alpha$	derivative with respect to $\alpha$
atmos	atmospheric property
ax	axial component
cg	about center of gravity
cyl	on cylinder
j	conditions in the jet
l	on lower surface
L	lift component
LE	about wing leading edge
max	maximum value

meas	measured value
N	normal component
u	on upper surface
0	total property
1	conditions upstream of the venturi
2	conditions at the venturi throat
$\infty$	free stream conditions

### Abstract

This wind tunnel study investigated the lift, drag, and pitching moment of a 20% thick, 8.5% camber, partial elliptical cross-section, single blowing slot, 2.325 aspect ratio, rectangular circulation control wing. The AFIT 5-foot wind tunnel was used. Lift and drag were referenced to the wind axis. The Reynolds number was  $5 \times 10^5$  for all tests. Angle of attack was varied from -6 to 16 degrees and the effects of pulsed blowing were investigated. Effects of tripping the Coanda jet with a small flow barrier attached spanwise along the Coanda surface were also studied. Results indicate that there is a limit on maximum lift obtainable by increasing circulation. The limit is presumed to be the result of three-dimensional effects. Pulsed blowing has little effect on average lift, but results in violent oscillation of the wing as the sting physically bends under cyclic loading. In certain situations, tripping the Coanda jet may reduce drag without decreasing lift.

## I. Introduction

### Background

Development of high lift devices for aircraft is of great importance. High lift techniques are required for V/STOL aircraft that can operate from short runways. High lift also allows steeper climb out of CTOL aircraft which decreases the size of the local area affected by aircraft noise. Military applications include the ability to operate from short improvised runways at Forward Operating Locations or damaged runways at established bases. Steep climb and descent also minimize vulnerability of tactical aircraft to enemy fire during takeoff and landing at forward locations.

Circulation control wings allow high lift coefficients without the complexity of mechanical high-lift devices. Circulation control wings also offer the possibility of building helicopter rotors that do not need to change angle of attack as they move from the advancing to the retreating side of the aircraft. The necessary modulation of lift coefficient may be accomplished simply by varying the amount of blowing.

The Kutta-Joukowski theorem states that: Ref. Keuthe and Chow (1):

$$\vec{L} = -\rho \vec{V}_\infty \times \vec{\Gamma} \quad (1)$$

where:

$$\Gamma = \oint_C \vec{V} \cdot d\vec{S} \quad (2)$$

$\Gamma$  = circulation about the closed curve  $C$

The amount of circulation and the free stream velocity determine the amount of lift generated by the airfoil. In thin airfoil theory,  $C$  is any closed curve that encircles the airfoil and  $\Gamma$  is defined as the circulation about the airfoil which is taken as positive in the counterclockwise direction. For a conventional airfoil, the amount of circulation is fixed by the angle of attack and the Kutta condition which states that an airfoil with a sharp trailing edge will generate enough circulation to fix the aft stagnation point at the trailing edge (1).

A circulation control airfoil has a blunt, typically circular trailing edge called the Coanda surface. A jet of high velocity air is blown over this surface such that the jet attaches to the surface by the Coanda effect. As the jet follows the surface around the blunt trailing edge, circulation and hence lift is increased. With no sharp trailing edge, the Kutta condition does not apply and the forward and aft stagnation points move closer together along the bottom of the airfoil. This movement of the stagnation



points is termed super-circulation (2). How far the stagnation points move is determined by the mass rate of flow and the velocity of the jet. In two dimensional potential theory, it would be possible to bring both stagnation points to the same location on the bottom of the airfoil with high enough blowing rates Kauthe and Chow (1).

Three dimensional wings behave much like airfoils except that downwash ( $w$ ) from the trailing vortex sheet tends to decrease effective angle of attack and thus lift. McCormick (1:51-64) states that in addition to the first order effect of downwash, the trailing vortex sheet must be deflected downward due to the Biot-Savart law. Consider a vortex filament that lies along the X-axis and starts at point (0,0) and extends to infinity in the positive X direction. The Biot-Savart law requires that for any point on the Y-axis:

$$w = \frac{\gamma}{4\pi r} \quad (3)$$

where:

$\gamma$  = strength per unit length of the vortex filament

and

$r$  = perpendicular distance from the vortex filament.

Now consider a vortex filament that extends to infinity in both directions:

$$w = \frac{\gamma}{2\pi r} \quad (4)$$

This requires a modification of conventional lifting line theory. Induced downwash velocity due to the trailing vortex sheet must be twice as much at a point infinitely behind the wing as at a point on the wing. Note that the wing is collapsed into a lifting line vortex. This difference in downwash velocity requires that the trailing vortex sheet be deflected downward. McCormick (3) shows that, using lifting line theory, this results in a limit on circulation induced lift of:

$$C_{Lmax} = 1.21 AR \quad (5)$$

McCormick then shows that, using the exact solution for an elliptic lift distribution, deflection of the vortex sheet results in a limit of:

$$C_{Lmax} = 0.855 AR \quad (6)$$

The limit on lift is not due to a breakdown of the Kutta-Joukowski theorem, but is due to the decrease in effective angle of attack which rotates the force vector in the free stream direction decreasing the lift component and

increasing the drag component.

It may be expected that elliptic planform circulation control wings will have maximum lift coefficients somewhere between these two limits. It was hoped to determine the performance of a rectangular planform wing relative to these limits.

### Previous Research

Considerable research has been done on two dimensional circulation control airfoils, most notable to this thesis, Walters, Myer, and Holt (4) who investigated steady and pulsed blowing of a cambered elliptical circulation control airfoil. Walters et al. found that higher lift coefficients could be obtained for a given blowing rate if the blowing air was pulsed at a frequency below 50 Hz. They found that frequencies above 50 Hz decreased lift.

Grumman Aerospace Corporation modified and flew an A-6 Intruder with a circulation control wing. (5) Lift was increased and landing speed was decreased, but maximum speed was reduced because of additional drag due to the blunt trailing edge. The horizontal stabilizer had to be enlarged and given inverse camber in order to offset the large nose down pitching moment of the circulation control wing.

Previous experimental work at AFIT has included, among others, a study by Harvell (6) who investigated multiple blowing slots on a two dimensional airfoil, Trainor (7) who showed it was feasible to test a sting mounted three dimensional wing in the AFIT five foot wind tunnel, Pelletier (8) who refined the methods of three dimensional testing in the AFIT tunnel.

### Present Study

This study expands the work of Pelletier (8) to higher blowing rates and angles of attack. The same model was used in the AFIT five foot wind tunnel, but Reynolds number was decreased from  $9 \times 10^5$  to  $5 \times 10^5$  to obtain data for higher blowing rates ( $C_\mu$ ) relative to free stream conditions. Lift, drag and moment coefficient data were obtained using a sting and 0.5 in. force balance. Wing surface pressure data were recorded and correlated with force balance data. Tufts were attached to the model to determine Coanda surface turning effectiveness and gauge the magnitude of three dimensional effects near the wingtips.

A pulser valve was manufactured and used to study the effects of pulsed blowing air on lift relative to blowing rate.

Three test runs were made with a flow trip attached to the Coanda surface to study the effects of forcing the jet to separate from the Coanda surface at a specific point.

## **II. Test Item Description and Instrumentation**

### **Wing Model**

The model used in this test was a 20-percent thick, 8.5 percent cambered, partial elliptic cross section, 2.325 aspect ratio rectangular wing with a single trailing edge blowing slot. The airfoil shape was similar to the models used by Harvell (6) and Trainor (7) and is shown in Figure 1. The low aspect ratio was selected to amplify three dimensional effects. The model consisted of two aluminum plenum chambers (left and right) separated by an aluminum sting mounting block. The bottom of the plenum chambers was the wing lower skin, which was flat between the wing nose piece and the Coanda surface, whereas the top of the wing was made using a fiberglass skin built up on top of the plenum chambers. Blowing air entered the model through a single removable 3/4 in. i.d. copper tube attached to a circular opening in the bottom of the wing at midspan. The opening was just behind the wing leading edge piece and forward of the sting mounting block. Two air distribution tubes inside the wing delivered air to the plenum chambers. Sections of 1/4 inch honeycomb inside each plenum chamber straightened the flow and reduced turbulence inside the model. The trailing edge slot was divided into a right and left slot with the sting mount between them. Planform of

the model is shown in Figure 2. The model was designed to remain within the limit for maximum chord to tunnel height of 0.25 proposed by Wood (9).

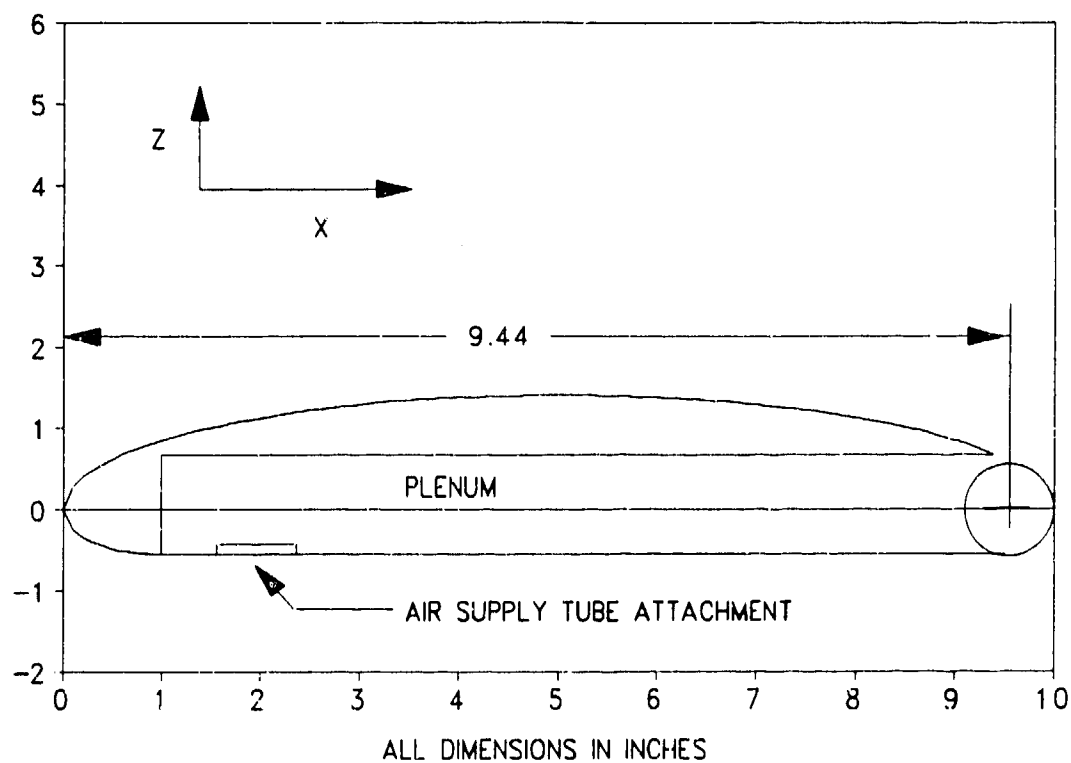


Figure 1. Circulation Control Wing Cross Section

The airfoil geometry was as follows:

*Upper Surface*

$$Z_u = 0.28\sqrt{25 - (5 - x)^2} \quad 0 \leq x \leq 9.44 \quad (7)$$

*Lower Surface*

$$Z_l = -0.56\sqrt{1 - (1 - x)^2} \quad 0 \leq x \leq 1 \quad (8)$$

$$Z_l = -0.56 \quad 1 \leq x \leq 9.44 \quad (9)$$

*Coanda Surface*

$$Z_{cyl} = \pm\sqrt{0.56^2 - (x - 9.44)^2} \quad 9.44 < x \leq 10 \quad (10)$$



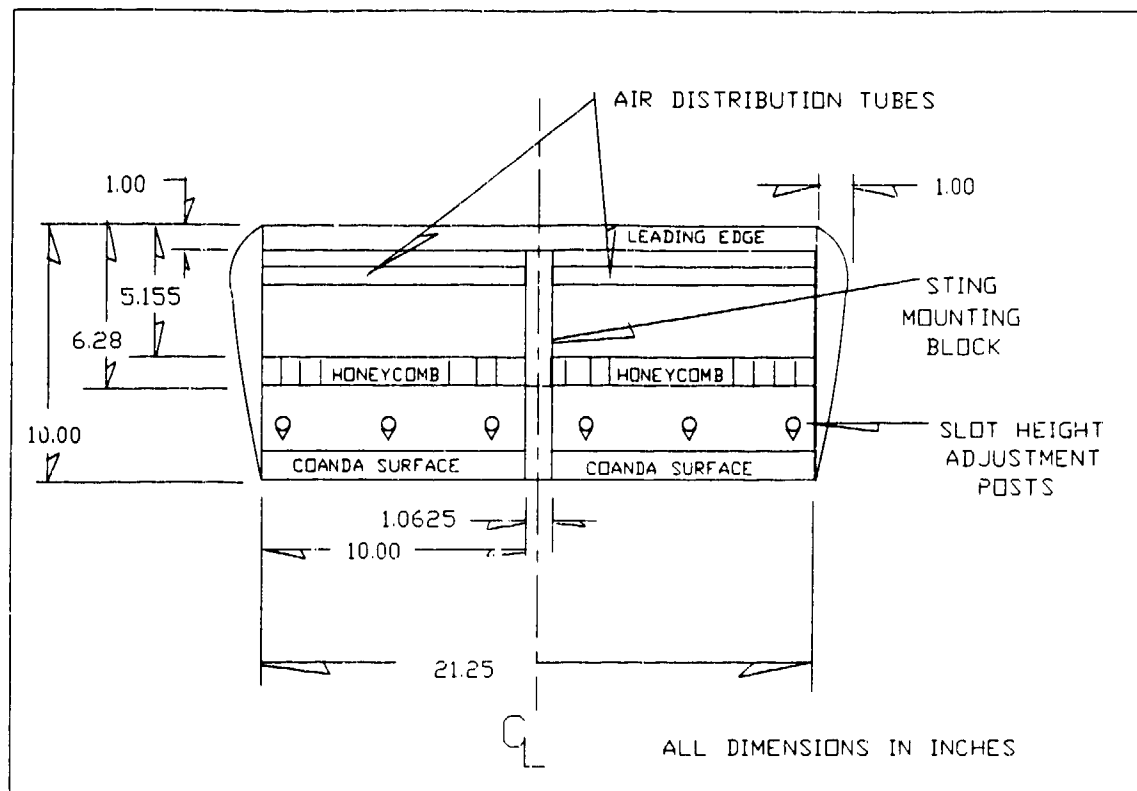


**Figure 2. Planform of Wing Showing Plenum Chambers, Honeycomb, Slot Height Adjustment Posts, Sting Mounting Block, and Coanda Surface**

The trailing edge/Coanda surface was designed according to Englar's work (10,11). The trailing edge radius to chord ratio was 0.056. Nominal slot height was 0.015 in. The slot height was slightly adjustable by means of six screws

which could be tightened to bend the plenum top skin down and decrease the slot height or loosened to allow the slot height to increase. These screws were adjusted independently to obtain uniform jet velocity spanwise across the slot.

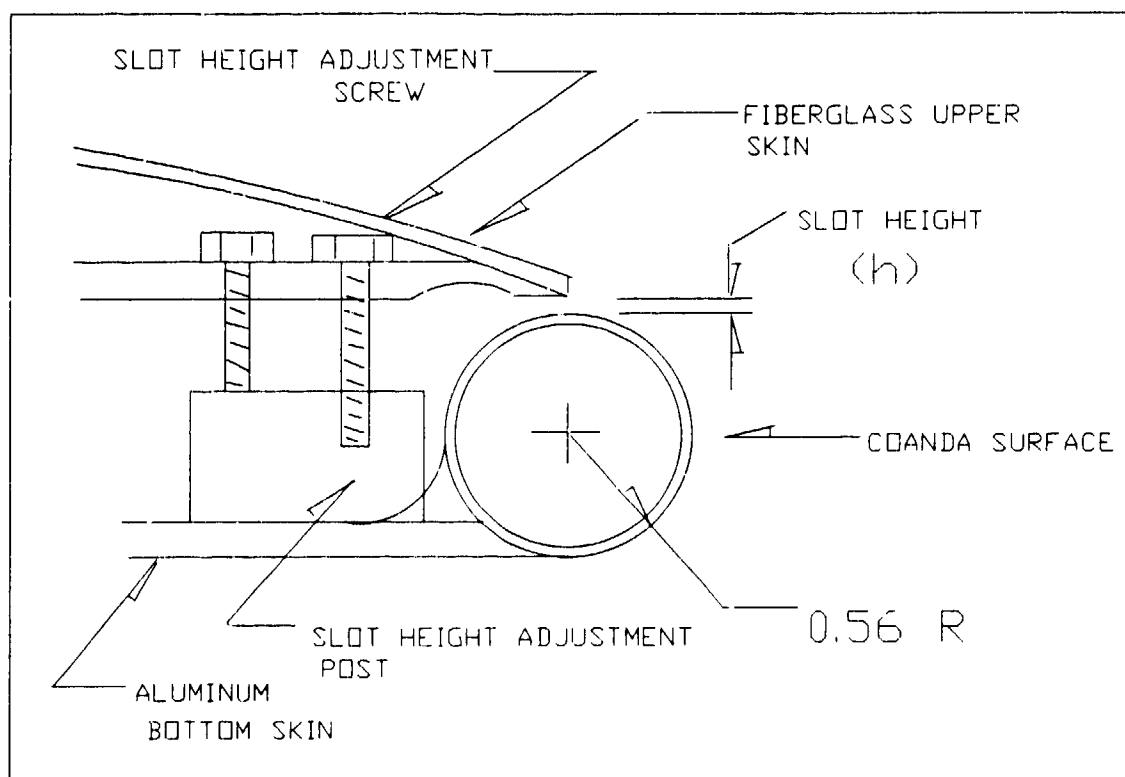


Figure 3. Detail of Blowing Slot, Coanda Surface, and Slot Height Adjustment Screws.

The wing was constructed to allow pressure measurements from both plenum chambers and at 56 points on the wing surface. One total pressure tube consisting of 3/64 in. stainless steel tubing was located in each plenum chamber and routed out of the model between the plenum chambers. Tubes for the 56 static pressure taps were routed along the top and bottom inside of the plenum chambers to minimize disturbance to the flow in the chambers.

A chromel-alumel thermocouple was installed inside the left plenum chamber to measure plenum total temperature. Temperature measurements were displayed on an Omega Engineering 415B digital thermocouple readout. Temperatures were recorded by hand.

Table 1. Static Pressure Port Locations \*

6 inches from left wingtip	10 inches from left wingtip	6 inches from right wingtip
x/c	x/c	x/c
0.00	0.00	0.00
0.025		
0.050		
0.10	0.10	0.10
0.20		
0.30	0.30	0.30
0.40		
0.50	0.50	0.50
0.60		
0.70	0.70	0.70
0.80		
0.90	0.90	0.90
0.94	0.94	0.94
0.97		
0.99		
1.00		

\* Ports were located on both the top and bottom of the wing at each position.

#### **Blowing Air Supply System**

Secondary air was supplied to the model from the base shop air system. The schematic is shown in Figure 4. Approximately 100 psia shop air was routed through a cyclone separator and filter system to remove condensation and oil.

A pressure regulator was installed at this point to regulate the amount of pressure available. The pressure regulator setting was held constant during testing. Downstream of the regulator, at the entrance to the Venturi flowmeter, was another chromel-alumel thermocouple connected to an Omega Engineering 415B digital thermocouple readout. This thermocouple was used to determine the static temperature of the secondary air entering the Venturi flow meter ( $T_1$ ). A screw valve located downstream of the thermocouple was used to vary flow rate during testing. The clean, dry air was passed through a 0.50 inch diameter Venturi flow meter. During preliminary testing of the model, The Venturi pressure taps ( $P_1$  at the entrance and  $P_2$  at the throat) were connected to 50 inch manometer tubes to read gage pressure. During wind tunnel testing, the manometers were replaced with calibrated Endevco 8530A-100 electronic pressure transducers referenced to atmospheric pressure. The transducer signals were amplified with Endevco 4423 signal conditioners powered by an Endevco 4225 power supply. The voltage readout was displayed on Hewlett Packard 3466A digital multimeters.

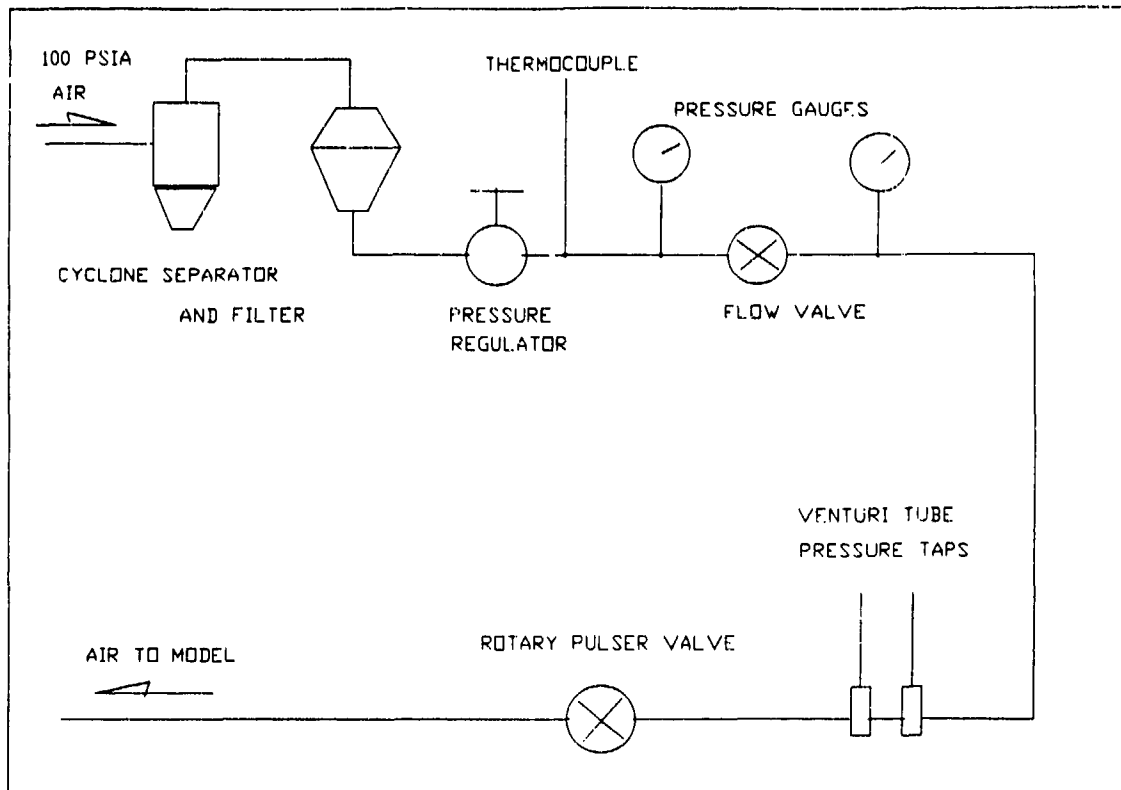


Figure 4. Secondary Air Supply

### Pulser Valve

It was desired to investigate the effects of pulsed blowing for this project. A pulser valve was designed after the kind used by Walters et al. (4). This rotary pulser valve, shown in Figures 5 and 10, consists of a cylindrical brass core with two intersecting air passages bored through

it. The air passages are perpendicular to the core axis and to each other. The brass core fits inside a hollow cylindrical steel casing with a single inlet port and outlet port. The core is spun by a direct current electric motor so that the air passages in the core alternately align with the ports in the casing. A seal is maintained by "O"-rings on either side of the air passages. The valve opens four times per revolution.

The core was designed so that the inside diameter of the casing is 5.22 times the radius of the air passages through the core. This geometric relationship causes one air passage to move out of alignment with the ports just as the other passage moves into alignment with the ports. This results in complete closure of the valve for only an instant between pulses. It was expected that this configuration would yield sinusoidal flow modulation.

The pulser was powered by a 1 horsepower Reliance Electric DC-1 motor controlled by a Reliance Electric DC1-70U controller. Pulsing rates between 8 and 80 Hz were possible. Clearance between the core and casing was minimal to prevent air leakage and the resulting high friction made the 1 horsepower motor necessary.

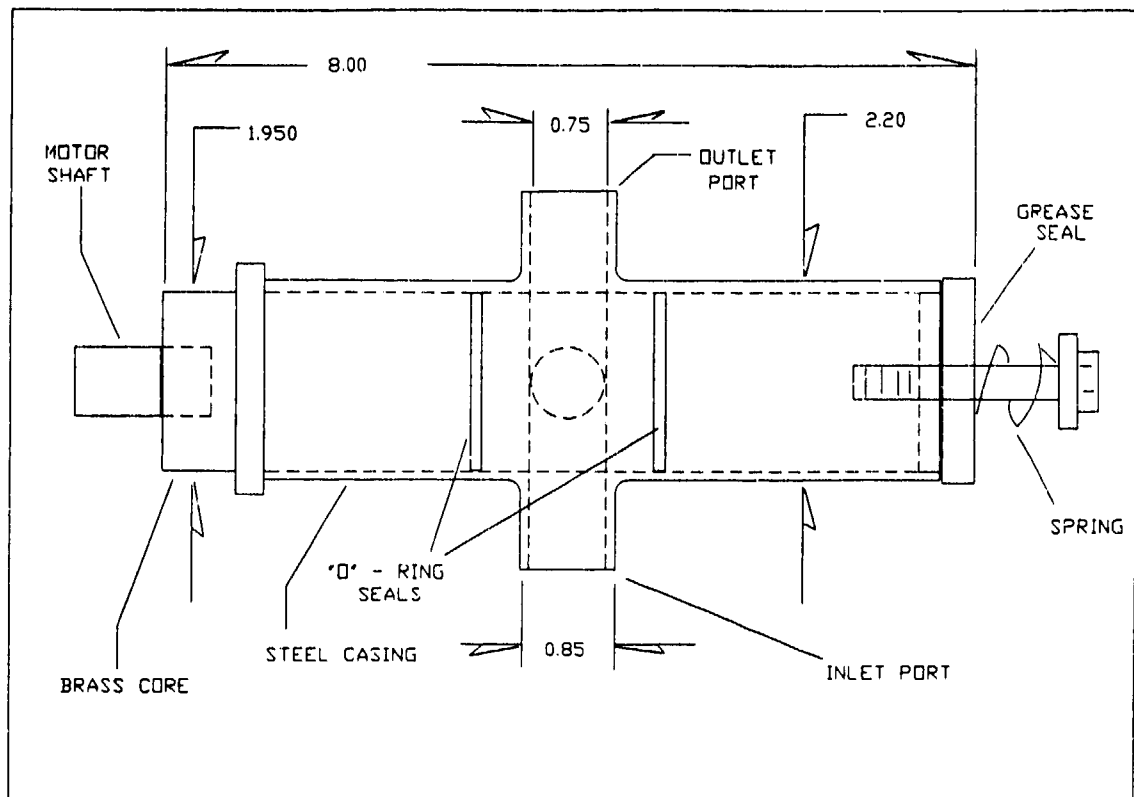


Figure 5. Pulser Valve

#### **AFIT 5-ft Wind Tunnel**

All testing was done in the AFIT 5-ft wind tunnel at Wright Patterson Air Force Base, Ohio. This tunnel is a closed test section, open circuit tunnel completely enclosed in a building specifically designed to enhance flow circulation. The tunnel is capable of wind speeds up to 200 mph. Flow is generated by two counterrotating 12-ft fans powered



by 4 DC motors. The test section is circular with a diameter of 5-ft. The tunnel contraction ratio is 3.7 to 1.

Tunnel total pressure is assumed to be atmospheric and static pressure is taken from a row of eight static ports located 2.5 feet from the tunnel mouth. Tunnel dynamic pressure (tunnel  $q$ ) is measured as the difference between atmospheric pressure and tunnel static pressure. Tunnel  $q$  is read from a water micromanometer and is also displayed as a voltage on a Fluke 8300A digital voltmeter which is connected to a Robinson-Halpern 157B-W125D-F-V31 "0 to 25 inches of water" precision electronic pressure transducer. The voltage output is recorded automatically by the tunnel data acquisition system during testing.

Model base pressure is measured from a total pressure tube attached to the sting several inches behind the model. This pressure tap is connected to a Robinson-Halpern 157B-W125D-F-V31 "0 to 25 inches of water" precision electronic pressure transducer and the voltage output is automatically recorded by the tunnel data acquisition system software during tests.

Tunnel temperature is recorded automatically by the tunnel data acquisition system software from a thermocouple located in the tunnel flow straightener vanes.

The AFIT wind tunnel has a turbulence factor of 1.5.

This factor is used to take into account the effects of the inlet guide vanes, fans, and tunnel wall vibration (10:147). Effective Reynolds number is defined as the Reynolds number of this test multiplied by the turbulence factor and should be used to compare results of this test to other tests conducted in different wind tunnels.

#### **Data Acquisition System and Force Balance**

The AFIT 5-ft wind tunnel data acquisition system consists of a Zenith Data Systems Z-300 computer with the wind tunnel data acquisition and data reduction software, a Hewlett Packard HP 3852A Data Acquisition Control Unit (DACU) and a Pressure Systems Inc. 780B/T Pressure Measurement System Data Acquisition and Control unit (DACU) with a 780B/T Pressure Calibration Unit (PCU) Trainor and Franke (16). The HP 3852A and 780B/T DACU are connected with the Z-300 through an IEEE-488 interface bus. All facets of data acquisition are controlled from the keyboard of the Z-300. A block diagram of the data acquisition system hardware is shown in Figure 6.

The HP 3852A DACU is used to interface the sting balance, angle of attack potentiometer, tunnel temperature thermocouple, tunnel  $q$  transducer, and base pressure transducer outputs with the tunnel data acquisition system.

The AFIT 5-ft wind tunnel has an Able Corporation Mark V force balance. This 0.5-in diameter, six-component, strain gauge type force balance is used to measure two normal force, two lateral force, one axial force component, and one rolling moment. Constant DC excitation voltage is provided to the balance by a Hewlett Packard 6205 regulated power supply. The data acquisition system automatically records voltages from each of the six strain gauges and resident software reduces the voltages to forces using a calibration matrix. The tunnel software is also capable of resolving the six forces on the balance into conventional lift forces, drag forces, and moments Systems Research Laboratories (13).

Angle of attack is determined from the voltage output of a position potentiometer physically connected to the sting. This voltage can be read from a Hewlett Packard 3466A digital multimeter and is recorded automatically by the tunnel data acquisition system software during tests. Information on calibration of the angle of attack transducer is in the section on Experimental Procedure - Calibrations.

The Pressure Systems Inc. 780B/T Pressure Measurement System was used to measure wing surface static pressures and plenum total pressures. This system is controlled by the 780B/T DACU which interfaces with the Z-300 through the IEEE-488 bus. Pressure taps in the wing were connected to

two Electronically Scanned Pressure (ESP) modules mounted at the base of the sting. A 3245B 45 psid module was used for pressure surface ports and plenum pressure tubes and a 3205B 5 psid module was used for suction surface ports. Plenum pressures above 5 psia were expected, but did not occur. Future tests should use a 5 psia ESP for pressure surface ports to increase accuracy. Plenum pressures above 5 psia should be measured with separate pressure transducers. Each ESP module has 32 pressure measurement ports - each with its own transducer, a calibration pressure port, two 100 psia pneumatic control ports, and a reference pressure port. The ESP modules were referenced to atmospheric pressure for this test. The PCU controls and provides on line calibration of the ESP modules. The PCU interfaces with the ESP modules both electronically and pneumatically. Reference Figure 6. The PCU is pneumatically connected to a 100 psia air bottle and a vacuum pump. The air bottle provides pressure for pneumatic switching of the ESP modules internal Calibrate/Measure valve and for positive calibration pressures. The vacuum pump provides vacuum for sub-atmospheric calibration pressures. Calibration pressures for each ESP module are preset with the PCU internal regulator valves. Precise measurement of the calibration pressures is done by quartz pressure transducers

within the PCU. Pressure data is transferred from the modules to the PCU electronically. The 780B/T DACU creates a second order polynomial calibration equation for each transducer (32 per ESP module) based on the transducer voltage outputs and calibration pressures.

$$P = C_0 + C_1V + C_2(V^2) \quad (11)$$

The coefficients  $C_0$ ,  $C_1$ , and  $C_2$  for each transducer are stored in the 780B/T memory and used for on line data reduction by the 780B/T DACU. The DACU is capable of outputting raw data (voltages) or engineering units (psi) to the Z-300. Calibration was done at the beginning of each test run. Reference (14) contains a complete description of the 780B/T system.

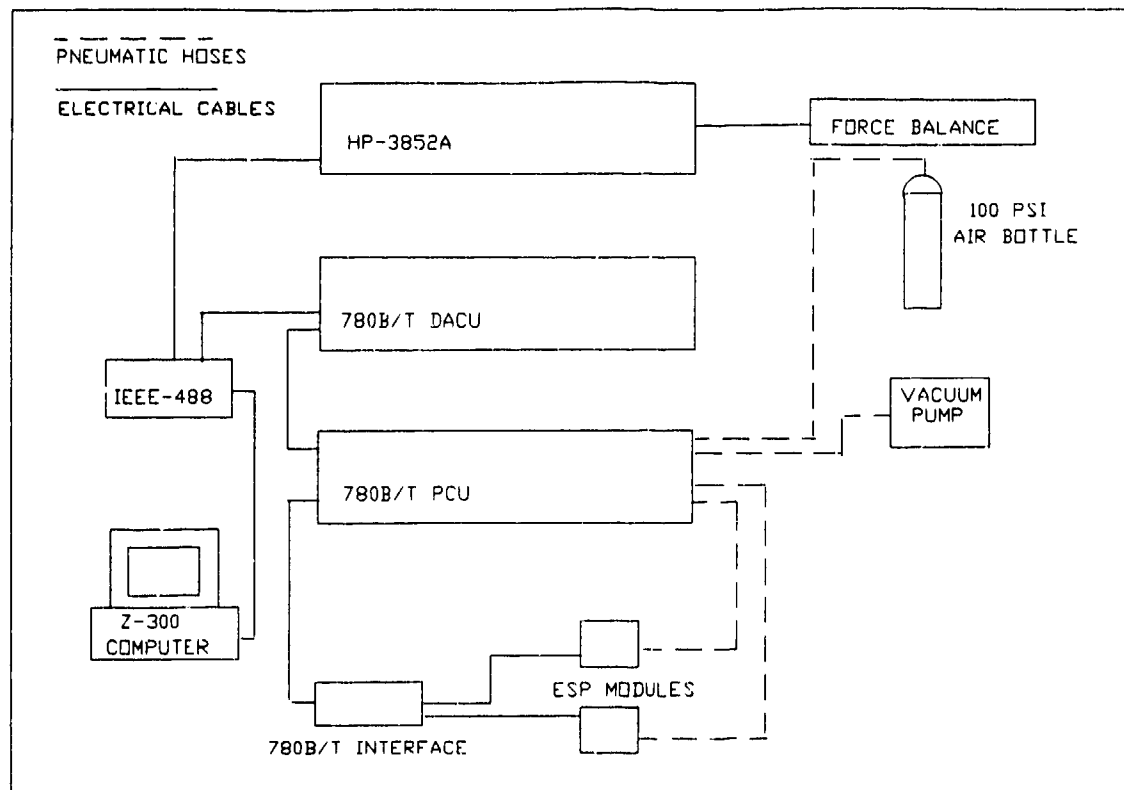


Figure 6. Data Acquisition System Hardware

### III. Experimental Procedure

#### Calibration

Several calibrations were performed prior to testing. The pressure transducers for the Venturi flow meter were calibrated by applying a known pressure and recording the output voltage. Linear regression analysis was used to determine the slope and intercept for the calibration equation for each transducer.

The force balance was calibrated by applying known loads to each of the six components. A special fixture was used to hang known weights from the balance. All components were loaded in both the positive and negative directions except the axial component which was only loaded positively. The normal components were loaded from 0 to 60  $\text{lb}_f$  in 10  $\text{lb}_f$  increments. The lateral components were loaded from 0 to 50  $\text{lb}_f$  in 10  $\text{lb}_f$  increments. The rolling moment component was loaded from 0 to 10  $\text{lb}_f$  in 2  $\text{lb}_f$  increments. The wind tunnel data acquisition software recorded strain gage voltages for each known load and created a calibration file for each component in each direction. An inclinometer was mounted on the sting and sting bend, in minutes of angle, was entered into the system software from the Z-300 keyboard. The system software was used to reduce the 11 calibration files (N1+, N1-, N2+, N2-, Y1+, Y1-, Y2+, Y2-, RM+, RM-, and AX+) to a single calibration matrix. The calibration matrix was applied by the system software to reduce the strain gage voltage output to loads during data reduction.

The file of sting bend values versus load (strain gage voltage) was used to correct angle of attack for sting bend due to load. This correction was done by the system software during data reduction.

The final calibration was to create a file of angle of attack versus voltage across the angle of attack potentiometer. The wing was mounted on the sting and an inclinometer was used to determine geometric angle of attack. Potentiometer voltage was recorded from an HP 3466A digital multimeter. The data was input to an angle versus volts file to be read by the system software during data reduction.

### Theory

Circulation control wings are compared based on a parameter called the momentum coefficient which is defined as:

$$C_\mu = \frac{\dot{m}_j V_j}{q_\infty S} \quad (12)$$

Momentum coefficient relates the momentum in the jet to the free stream dynamic pressure and is nondimensionalized with the wing planform area.

To compute  $C_\mu$  it is necessary to know  $V_j$  and the jet mass flow rate as well as the free stream dynamic pressure. It is typically assumed that because the expansion is sudden, occurring in a very short duct, the jet expands isentropically to the free stream static pressure. From the isentropic relations:

$$\frac{T_0}{T} = 1 + \frac{\gamma - 1}{2} M^2 \quad (13)$$



$$\frac{P_0}{P} = \left( 1 + \frac{\gamma-1}{2} M^2 \right)^{\frac{\gamma}{\gamma-1}} \quad (14)$$

$$M^2 = \frac{V^2}{\gamma R T} \quad (15)$$

The jet velocity may be written as:

$$V_j = \left\{ 2RT_0 \frac{\gamma}{\gamma-1} \left[ 1 - \left( \frac{P}{P_0} \right)^{\frac{\gamma-1}{\gamma}} \right] \right\}^{1/2} \quad (16)$$

For model checkout and jet thrust runs with the wind tunnel off, The pressure the jet expands to (P) was taken to be  $P_{atmos}$ . For the actual tests with the wind tunnel on, P was taken as  $P_{atmos}$  minus the corrected free stream dynamic pressure which can be written using the corrected free stream Reynolds number as:

$$P = P_{atmos} - 1/2 \frac{(Re\mu)^2 R T_{atmos}}{P_{atmos} C^2} \quad (17)$$

and:

$$q_\infty = P_{atmos} - P \quad (18)$$

Mass flow rate was measured with a calibrated Venturi meter. According to Doebelin (15):

$$\dot{W} = C_d A_2 \sqrt{\frac{2g\gamma P_1}{(\gamma-1)v_1}} \sqrt{\frac{(P_2/P_1)^{2/\gamma} - (P_2/P_1)^{\frac{\gamma+1}{\gamma}}}{1 - (A_2/A_1)^2 (P_2/P_1)^{2/\gamma}}} \quad (19)$$

Which reduces to:

$$\dot{m} = C_d A_2 P_1 \sqrt{\frac{2\gamma}{RT_1(\gamma-1)}} \sqrt{\frac{1 - PR^{\frac{\gamma-1}{\gamma}}}{PR^{-2/\gamma} - AR^2}} \quad (20)$$

For the Venturi used in this test:  $C_d = 0.970$ ,  $A_2 = 0.001362 \text{ ft}^2$ , and Area Ratio,  $AR = A_2/A_1 = 0.3677$ .  $PR$  is the Venturi Pressure Ratio  $P_2/P_1$  measured from the Venturi pressure taps.

Prior to each test run, atmospheric temperature was read from a mercury thermometer and atmospheric pressure was read from a Henry J. Green ML-330/FM mercury barometer and the desired tunnel  $q$  was determined from:

$$q_\infty = 1/2 \frac{(Re\mu)^2 RT_{atmos}}{P_{atmos} C^2} \quad (21)$$

Where Reynolds number was determined by the test plan. Tunnel  $q$  was converted to inches of water and set by the tunnel operator.

#### Model Checkout

This study used Pelletier's model (8) which had been damaged during removal from the sting balance. After the model was repaired, it was necessary to confirm that all pressure ports were open and that the tubes were correctly labeled. This was done by spreading leak detection fluid (watered down detergent) over each port and applying air pressure to the corresponding tube. Bubbling of the leak

detection fluid verified that the port was not clogged and was correctly labeled.

The model was checked for air leaks by installing the copper blowing air supply tube on the model and connecting the hose from the secondary air system. Secondary air was turned on and the model checked for leaks by feeling for stray air jets and spreading leak detection fluid over seams and fastener holes. Leaks were detected around the wingtip fastener holes. The fasteners were removed and reinstalled wet with silicone Room Temperature Vulcanizing (RTV) sealant. The leaks were eliminated.

#### Preliminary Testing

The blowing slot was adjusted to a nominal height of 0.012 inches with a feeler gauge by turning the slot height adjustment screws. Pelletier (8) had used a nominal slot height of 0.015 inches, but it was hoped to increase plenum pressure and thus jet velocity by constricting the slot. Uniform jet velocity along the slot was desired to ensure uniform jet attachment to the Coanda surface. With the model mounted on a bench outside the tunnel, a fixture was attached to the model so that a pitot tube could be mounted immediately aft of the blowing slot to measure jet total pressure at any point along the trailing edge. The pitot tube was connected to a 50 inch mercury manometer referenced

to atmospheric pressure. The total pressure was measured at 0.50 inch intervals spanwise along the slot for a mass flow rate of 0.004295 slugs/sec. This was the highest flow rate that could be maintained for a long enough time to complete the jet velocity survey. The velocity profile is presented in Figure 7. With the slot height set at 0.012 inches, the jet was not very uniform and very slight adjustments to slot height on one side of the wing had significant effects on the jet on the opposite side.

The slot height was adjusted with secondary air on in an attempt to improve the uniformity of the jet. The final adjusted slot height varied from 0.012 to 0.018 in. The velocity profile for the adjusted slot height with a total mass flow rate, measured through the Venturi flow meter, of 0.004081 slugs/sec is presented in Figure 8.

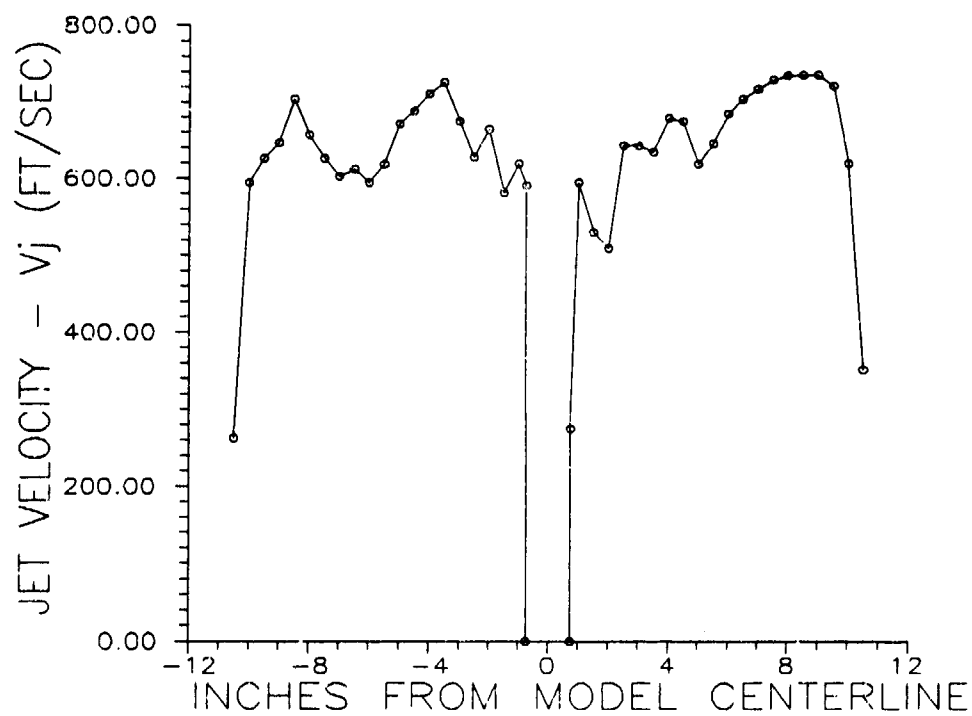


Figure 7. Initial Jet Velocity Profile with mass flow rate  $\dot{m} = 0.004295$  slugs/sec, Wind Off.

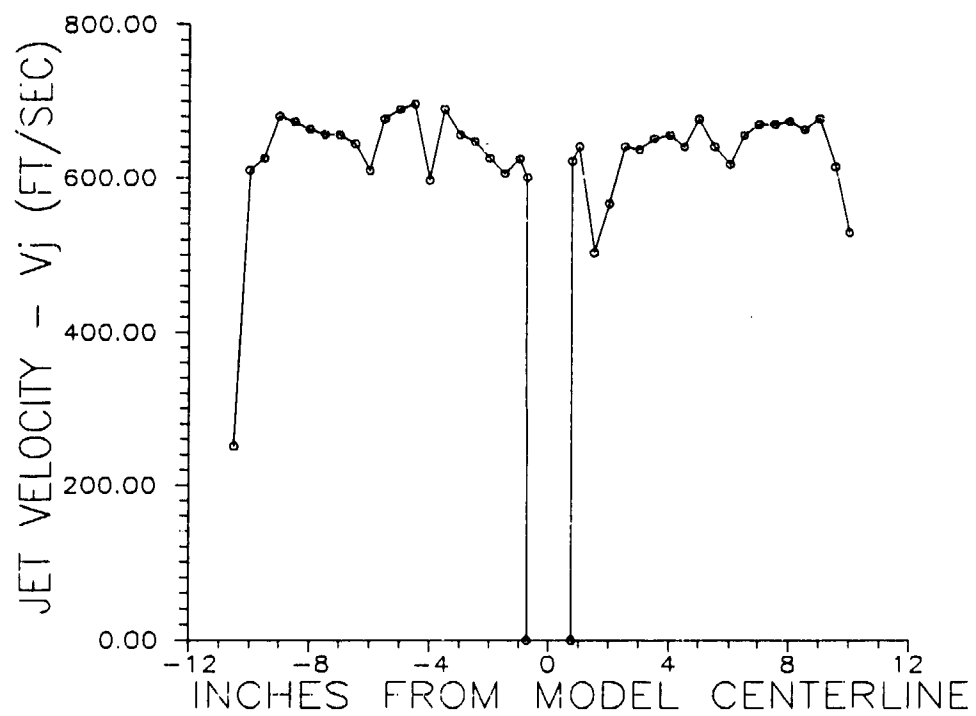


Figure 8. Jet Velocity Profile After Adjustment with mass flow rate  $\dot{m} = 0.004081$  slugs/sec, Wind Off.

The blowing air tube was removed from the model and the hole covered with a flush mount fairing. The model was mounted on the sting balance and the pressure tap tubes connected to the ESP modules. The tubes were wrapped with tape to secure them to the sting. The electrical and pneumatic connections for the ESP modules were routed out of the tunnel through a 1.0 inch diameter hole in the bottom of the tunnel test section aft of the model. The hole was sealed with tape. The plenum chamber thermocouple leads were routed along the sting and out of the tunnel with the ESP connections.

A tare run was performed with the clean wing (blowing tube, fairing, and hose not installed). The wing was moved through a range of angles of attack with the tunnel wind off while voltages registered by the balance strain gages were recorded by the tunnel data acquisition software. These values are subsequently used by the tunnel software to eliminate the model weight from forces calculated during data reduction.

A test run is defined as several data acquisition points with a single parameter varied and all others held constant. A test run was performed on the clean wing at Reynolds number =  $5 \times 10^5$ . Angle of attack was varied from -6 to +16 degrees, in two degree increments, as determined by the

angle of attack voltmeter. Actual values differ slightly due to the sting bending under load, which is taken into account during data reduction. The baseline values of  $C_L$ ,  $C_D$ , and  $C_{MLE}$  for the clean wing were used to correct  $C_L$ ,  $C_D$ , and  $C_{MLE}$  values measured with blowing tube and hose installed and to compensate for sting bend. See section IV. Data Reduction. These values are plotted in Figures 11 to 13.

The 9 in. long copper blowing air tube was installed on the bottom of the model. The tube was attached just behind the leading edge so that it extended aft to the trailing edge. Silicone RTV sealant was used to prevent leaks. One inch o.d., 0.75 in. i.d. plastic hose was used to connect the tube to the secondary air system. The hose was loosely secured to the sting with tape. The hose entered the tunnel through a 1 inch diameter hole above and aft of the model. The pulser was not in line. A fiberglass fairing was installed over the blowing air tube. Photos of the model installed in the tunnel with the blowing tube, hose and fairing installed are presented in Figures 9 and 10.

Another tare run was performed with the blowing air tube installed and the hose connected.

A test run was performed with no blowing. Angle of attack was varied from -6 to +16 degrees in two degree

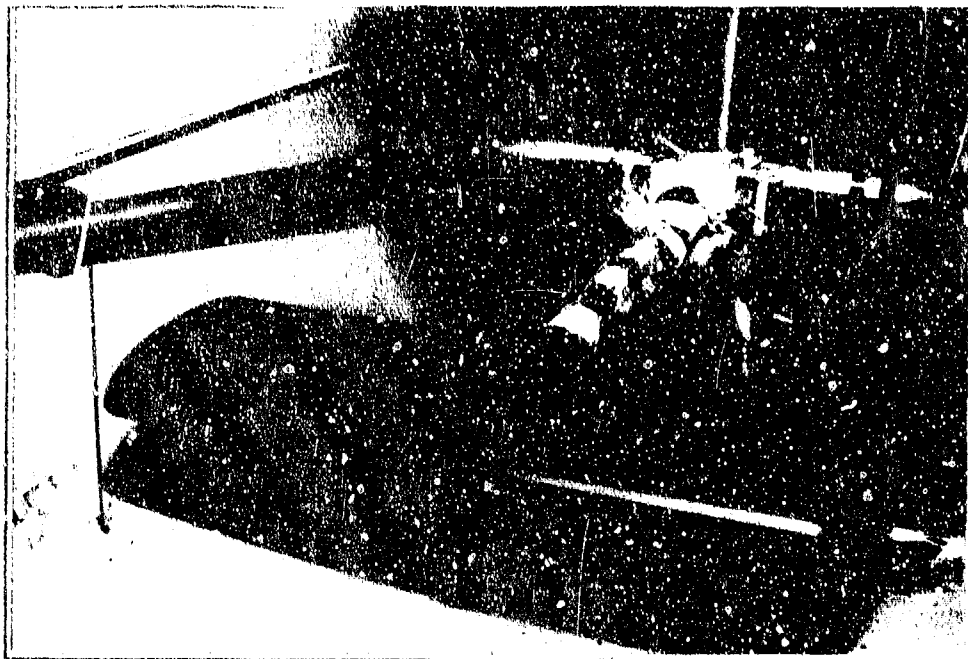


increments. Aerodynamic coefficients from this run are compared to those of the clean wing in figures 11 to 13.

The aerodynamic interference of the blowing tube, hose, and fairing had minimal effect on lift coefficient.  $C_L$  values were slightly higher for the clean wing.  $C_D$  was increased as much as 15 percent by the presence of the blowing tube, hose, and fairing.  $C_{MLE}$  remained negative and  $dC_{MLE}/d\alpha$  became more negative with the blowing tube, hose, and fairing attached.

A test run was performed with blowing, but the wind tunnel off to determine the normal and axial forces due to the jet thrust. Secondary air was varied from maximum to minimum available in 20 steps with data taken at each point. The tunnel software was used to resolve the jet thrust into axial and normal components. Axial and normal jet thrust are plotted in Figures 14 and 15. The axial force was always in the negative drag (positive thrust) direction. The normal force was either negative or positive depending on the jet mass flow rate. At low mass flow rates, the jet did not remain attached to the Coanda surface and the normal force was in the negative lift direction. At higher mass flow rates, the jet remained attached further around the Coanda surface and the normal force was in the positive lift direction. There was considerable scatter in the data, but

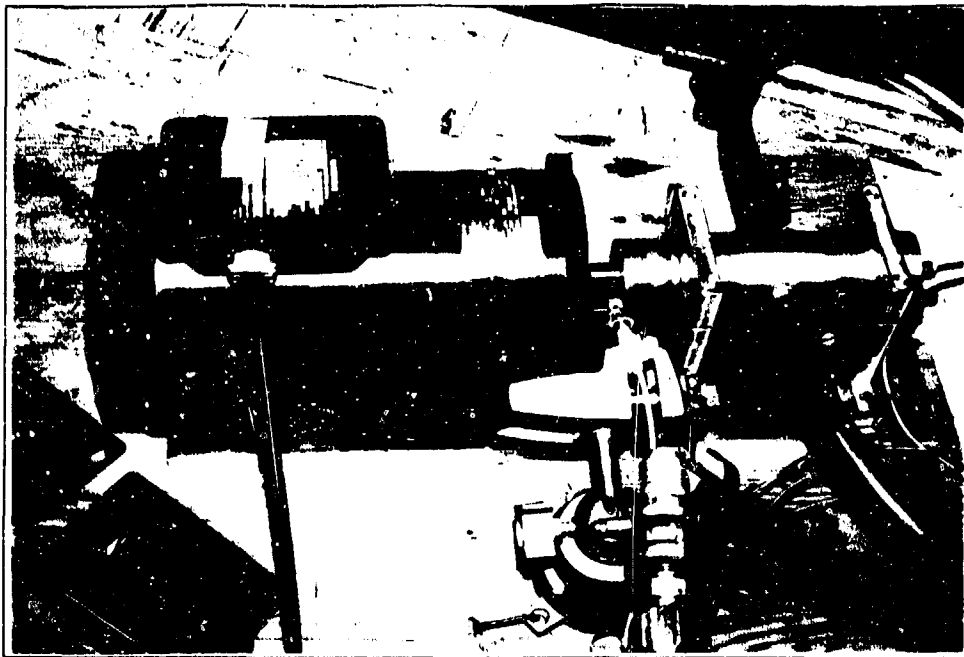
since the jet thrust correction was an order of magnitude smaller than sting bend corrections it was deemed acceptable to approximate the axial and normal forces linearly. More detail on how this data was used to correct measured values of  $C_L$  is in section IV. Data Reduction.



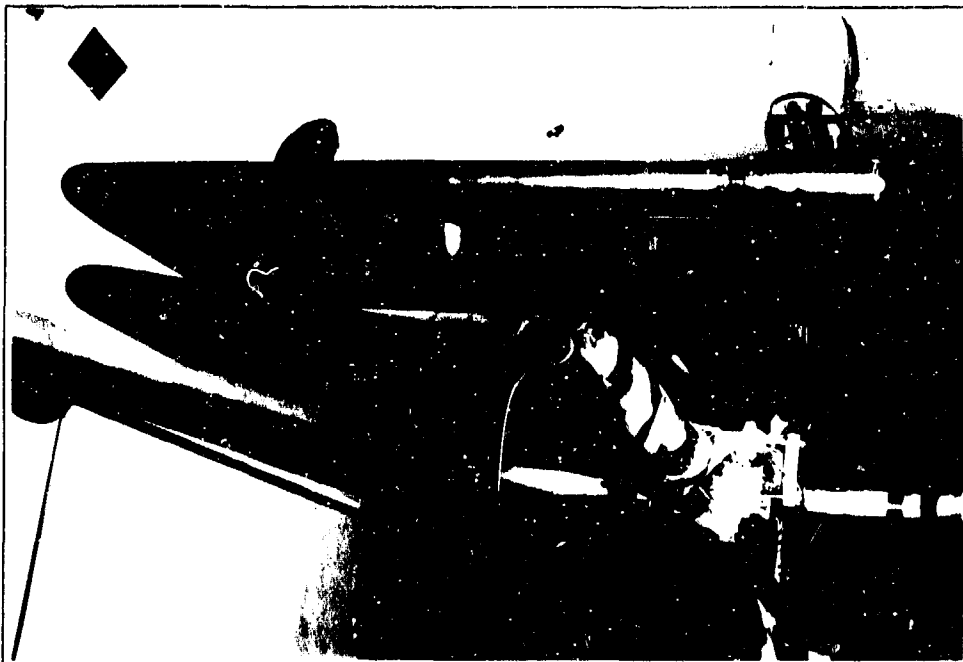
Looking down and aft.



Looking down and forward.  
Figure 9. Two Views of the Wing Mounted on Sting.



1 Hp DC motor and pulser valve.



Looking up and aft.  
Figure 10. Pulser Valve/Motor and Wing Mounted on Sting.

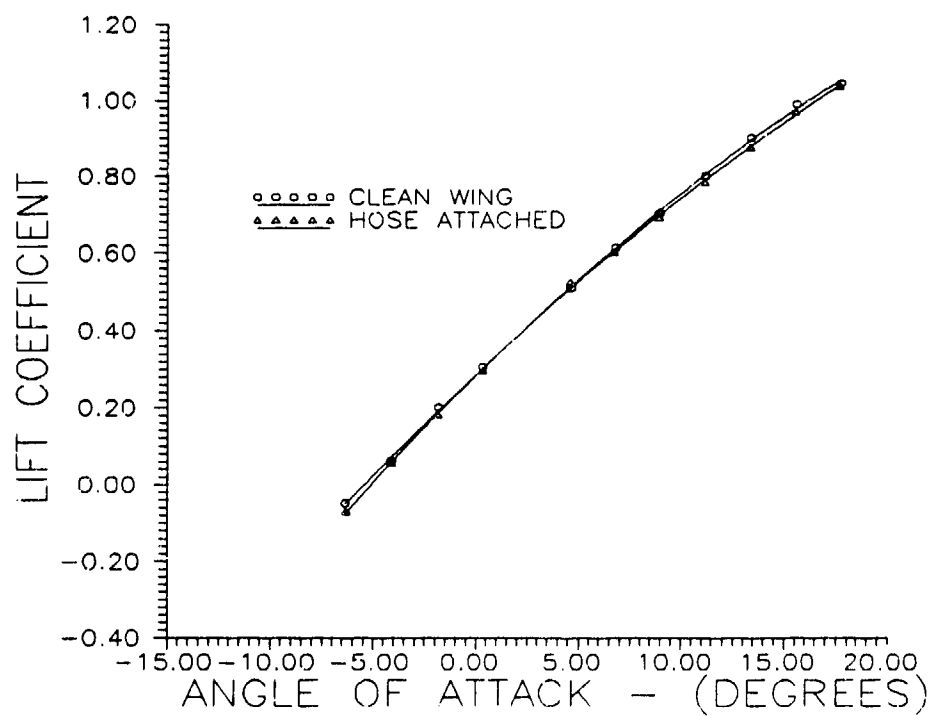


Figure 11. Wing Basic Lift Coefficients at  $Re = 5 \times 10^5$

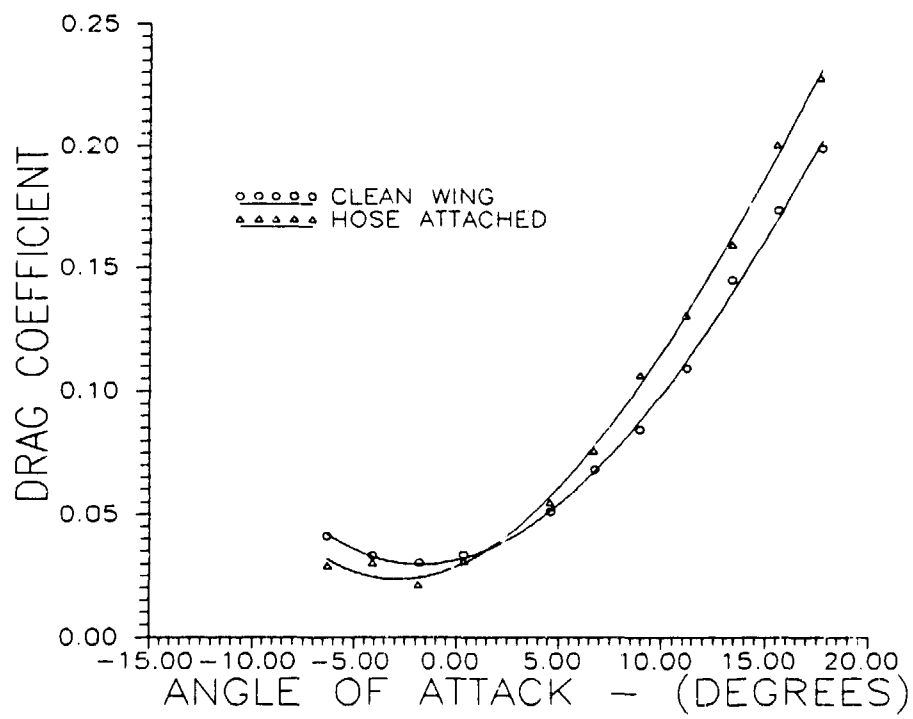


Figure 12. Wing Basic Drag Coefficients at  $Re = 5 \times 10^5$

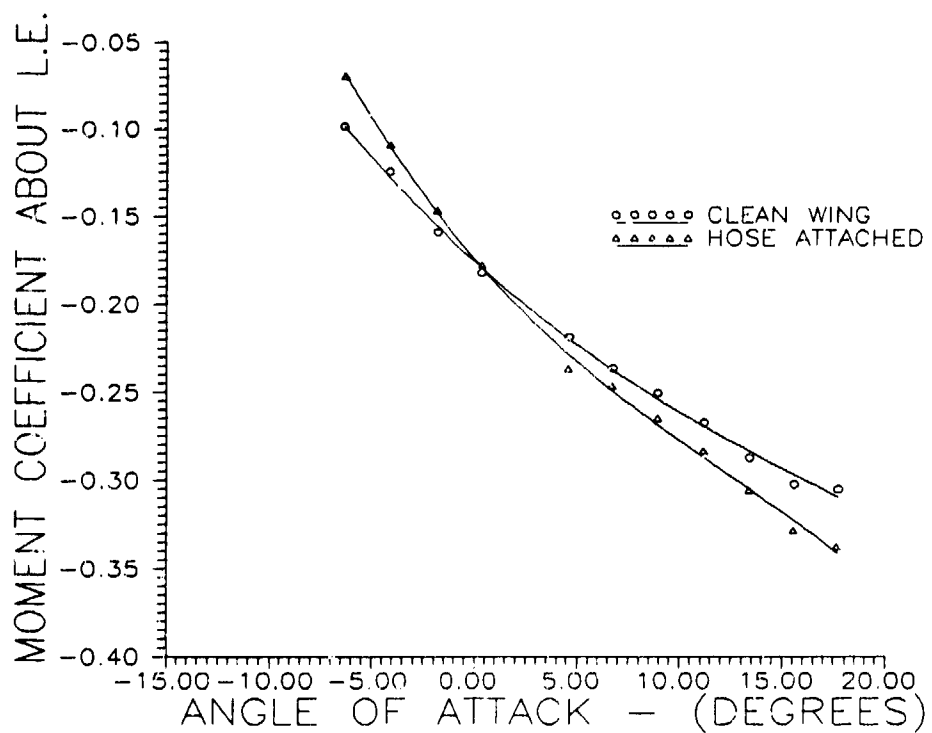


Figure 13. Wing Basic Moment Coefficients at  $Re = 5 \times 10^5$

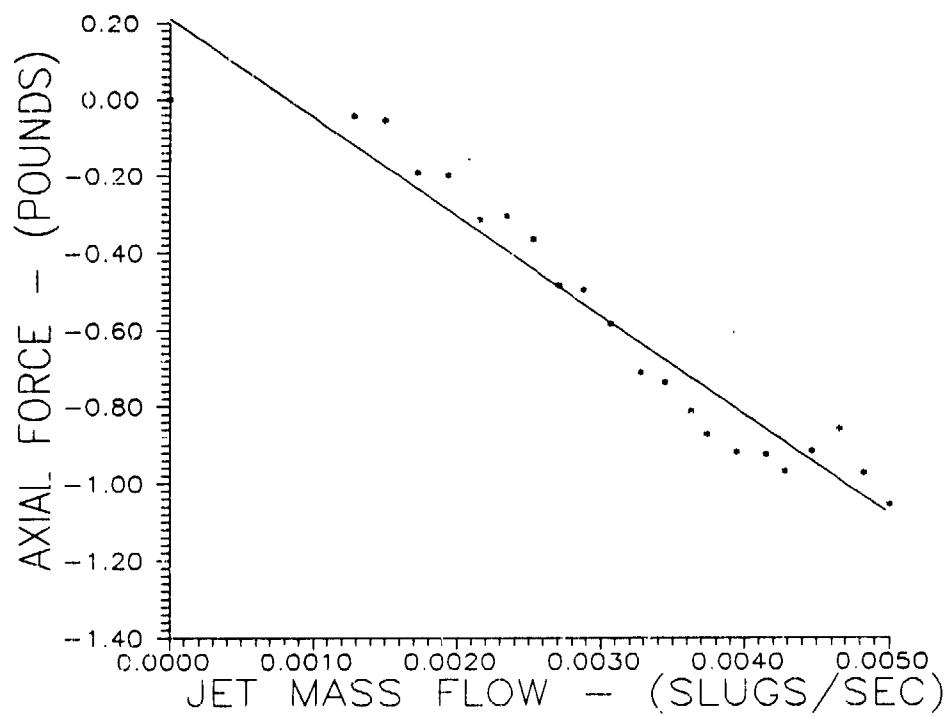


Figure 14. Axial Force Due to Jet Thrust



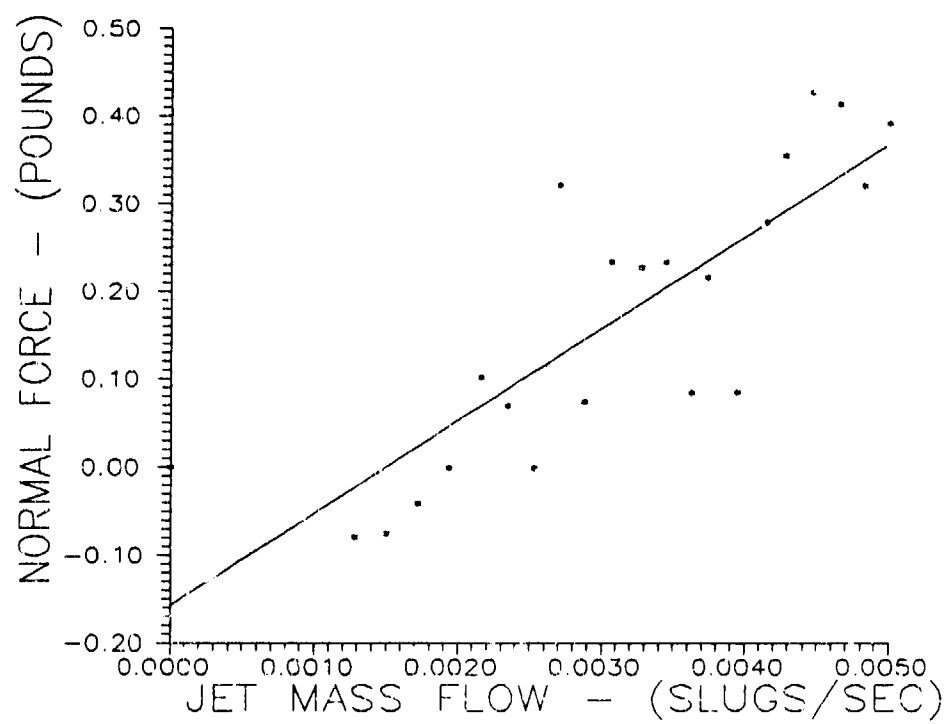


Figure 15. Normal Force Due to Jet Thrust

The voltage output from the Venturi flow meter pressure transducers was teed to a Tektronix 465M Oscilloscope so that dynamic flow rate could be observed with the pulser valve operating. It was verified that the voltage readout of the digital multimeters was the same as the mean voltage displayed on the oscilloscope for frequencies up to 80 Hz. It was therefore determined that mass flow rates calculated using the digital multimeter readouts were mean flow rates. It was found that for frequencies below 10 Hz the mass flow rate appeared sinusoidal about a mean flow rate. The amplitude of the oscillation was approximately 70 percent of the mean value. The amplitude decreased with increasing frequency and the valleys became sharper. Above 16 Hz the valleys were very sharp and the oscilloscope trace of the flow rate appeared to be the absolute value of a sine wave superimposed on the mean flow rate. Beyond 25 Hz the amplitude remained constant at approximately 22 percent of the mean flow rate. The character of the oscillation remained that of the absolute value of a sine wave superimposed on a mean flow rate. Flow rates and momentum coefficients for the pulsed runs are mean values calculated from the digital multimeter readouts.

### Primary Testing

All tests were run at a nominal Reynolds number of  $5 \times 10^5$ . This corresponded to a tunnel  $q$  between 2.0 and 2.2 inches of water. There were three series of test runs made for this study. The objective of these test runs was to determine lift, drag and pitching moment characteristics of the circulation control wing for both steady and pulsed blowing.

Steady blowing runs were made at angles of attack from -6 degrees to +16 degrees in 2 degree increments except for 8, 10, and 14 degrees. These runs were made to establish the baseline performance of the wing and to extend the work of Pelletier (8) to higher momentum coefficients.

For these runs, the momentum coefficient was varied manually by adjusting the flow valve from maximum flow to minimum flow in 20 steps with a data point taken at each step. For each data point, the tunnel data acquisition system was used to record force balance and pressure measurement system data. Venturi pressure transducer voltages, plenum thermocouple, and Venturi  $T_1$  thermocouple readouts were recorded manually. Atmospheric temperature and pressure were recorded prior to the beginning of each run. The ESP modules were calibrated automatically at the start of each run. Flow conditions were allowed to stabi-

lize for one minute at each blowing rate before data was taken.

The second series of runs was made with a 3/32 inch diameter piece of cord bonded spanwise across the Coanda surface to act as a flow trip. The cord was attached at a point 135 degrees from the top of the cylindrical section trailing edge. The cord is very nearly the diameter of the Coanda jet thickness, as measured during model checkout, and was expected to force the jet to separate if it had not separated prior to reaching the flow trip. Flow visualization using tufts indicated that the jet normally separates near this point and that the trip did force the jet to separate at angles of attack and jet mass flow rates where it would otherwise have remained attached beyond this point. It was hoped to determine if the Coanda jet was remaining attached beyond the Coanda surface and causing a suction zone on the bottom of the wing and thereby decreasing lift.

The jet-tripped runs were performed the same way as the steady blowing runs discussed above. Runs were made at 0, +6, and +16 degrees angle of attack.

The final series consisted of pulsed blowing runs. For these runs, blowing rate was held as close to constant as possible while the pulsing frequency was varied. Three runs were made, one each at a high, medium, and low blowing rate.

Data recording was similar to previous runs with pulsing frequency recorded manually. An Industrial Solid State Controls Incorporated 9918-29 transducer and 1262-1LCB motion detector signal conditioner connected to a Hewlett Packard 5316A universal counter was used to determine the rotational frequency of the pulser valve. Pulsing frequency was 4 times the rotational frequency because the valve opens 4 times per revolution.

#### IV. Data Reduction

##### Momentum Coefficient

A computer program was written to calculate blowing mass flow rate, jet velocity, and momentum coefficient. The program uses equations 12, 16, 20, and 21 with atmospheric temperature and pressure, Venturi flow meter pressures  $P_1$  and  $P_2$ , Venturi temperature  $T_1$ , and plenum chamber total temperature input by the user.

##### Wind Tunnel Corrections

The wind tunnel data reduction software automatically applies several corrections to the data. These corrections are performed according to the methods of Pope (12).

Solid blockage causes the streamlines to curve around the model and to be squeezed together due to the proximity of the tunnel walls. The resulting increase in effective dynamic pressure tends to increase forces on the model.

Buoyancy refers to the thickening of the boundary layer along the walls of the tunnel. The effect of the thickening boundary layer is an effective decrease in the cross-sectional area of the tunnel and an acceleration of the flow. The result is a reduced pressure downstream which tends to increase drag force.

Wake blockage occurs because the fluid in the wake moves more slowly than in the free stream and tends to block the flow. Continuity requires that the free stream accelerate around the wake blockage resulting in a favorable pressure gradient and increased drag force.

Downwash correction is required because the tunnel walls tend to attenuate downwash and decrease induced drag.

It has been found in prior tests that the dynamic pressure calculated from the static ports at the mouth of the tunnel vary from measured tunnel  $q$  in the test section by a factor of 1.019 Systems Research Laboratories (13). This "skew" factor was applied to the data from this study.

Standard wind tunnel corrections have been found to be valid for circulation control airfoils as long as lift coefficient is less than 4 and chord length is less than  $1/3$  of the tunnel width Walters et al. (4). These conditions were met by this test.

### Lift Coefficient

The wind tunnel data reduction software automatically reduces the force balance strain gage outputs to forces and resolves the forces into lift, drag, and pitching moment about the center of gravity of the model Systems Research Laboratories (13). Weight tares are applied to eliminate the weight of the model. The software also reduces these forces into coefficients based on the corrected dynamic pressure and planform area of the model.

For this test, lift coefficient relative to the wind axis and corrected for tunnel effects was output from the data reduction software and is referred to as the measured value. The first correction applied was for the effect of the blowing tube and hose attachment. Lift coefficient versus angle of attack was plotted for the clean wing and for the wing with blowing tube and hose attached without blowing. See Figure 11. Both lift curves were approximated with third order polynomials of the form:

$$Y = C_0 + C_1 X + C_2 X^2 + C_3 X^3 \quad (22)$$

With  $Y = C_L$  and  $X = \text{Angle of attack}$ . For any given angle of attack, both equations could be solved and the hose attached solution subtracted from the clean wing solution to obtain an additive correction to the measured lift coefficient at that angle of attack. This was done for every data point

from each test run.

The sting bend correction was used to correct measured lift coefficients for the fact that actual angle of attack varied from desired angle of attack because of the sting bending under load. The polynomial equation for lift coefficient of the clean wing was solved for both the desired angle of attack and the actual angle of attack. The actual angle of attack solution was subtracted from the desired angle of attack solution to yield an additive correction.

The final correction to lift coefficient was for thrust created by the jet. Because the forces were very small relative to typical lift values and the data was not particularly well behaved, these forces were approximated by linear equations. See figures 14 and 15. Lift force due to jet thrust is given by:

$$F_L = F_N \cos \alpha - F_{ax} \sin \alpha \quad (23)$$

and:

$$\Delta C_L = \frac{F_L}{q_\infty S} \quad (24)$$

Delta  $C_L$  due to jet thrust is then subtracted from the measured lift. Typical  $C_L$  corrections are less than 6 percent, with hose corrections accounting for 0.5 percent,



sting bend 4.5 percent, and jet thrust 2 percent. The hose correction is in the opposite direction of sting bend and jet thrust. Table 2 contains typical  $C_L$  corrections.

Table 2. Typical Lift Corrections

Nominal Angle of Attack = +6 Degrees

Re =  $5 \times 10^5$

Measured Alpha	$C_L$	$C_{mu}$	Corrections			Correct $C_L$
			Hose	Sting Bend	Jet Thrust	
7.38	1.4181	0.1793	0.0073	-0.0629	-0.0275	1.3350
7.37	1.4017	0.1742	0.0073	-0.0625	-0.0266	1.3199
7.33	1.3602	0.1602	0.0072	-0.0607	-0.0251	1.2816
7.32	1.3404	0.1522	0.0072	-0.0602	-0.0238	1.2636
7.31	1.3272	0.1450	0.0072	-0.0598	-0.0227	1.2520
7.27	1.2805	0.1323	0.0071	-0.0580	-0.0211	1.2085
7.26	1.2640	0.1232	0.0071	-0.0575	-0.0197	1.1939
7.24	1.2353	0.1164	0.0071	-0.0566	-0.0184	1.1673
7.24	1.2327	0.1079	0.0071	-0.0566	-0.0173	1.1659
7.21	1.1901	0.0987	0.0070	-0.0553	-0.0158	1.1260
7.19	1.1770	0.0915	0.0070	-0.0544	-0.0144	1.1152
7.18	1.1567	0.0824	0.0070	-0.0539	-0.0129	1.0968
7.13	1.1232	0.0760	0.0069	-0.0516	-0.0119	1.0665
7.14	1.1048	0.0678	0.0069	-0.0521	-0.0104	1.0491
7.11	1.0749	0.0601	0.0068	-0.0507	-0.0090	1.0219
7.06	1.0197	0.0524	0.0067	-0.0485	-0.0076	0.9704
7.04	0.9844	0.0446	0.0067	-0.0476	-0.0061	0.9374
7.02	0.9408	0.0371	0.0067	-0.0467	-0.0046	0.8962
6.97	0.8713	0.0301	0.0066	-0.0444	-0.0031	0.8303
6.93	0.8318	0.0225	0.0065	-0.0426	-0.0014	0.7943
6.88	0.7659	0.0157	0.0064	-0.0403	0.0002	0.7322
6.72	0.5950	0.0000	0.0061	-0.0330	0.0097	0.5778

### Drag Coefficient

Drag coefficient corrections are similar to lift coefficient corrections, but there is no correction for jet thrust. Equations of the form of eq. 22 were derived for drag coefficient as a function of angle of attack for both the clean wing and the wing with blowing hose attached. See Figure 12. Corrections for the hose being attached and for angle of attack deviating from the desired angle of attack were done in the same manner as for lift coefficient.  $C_D$  is not normally corrected for jet thrust, instead Equivalent Drag is used. Typical  $C_D$  corrections were less than 15 percent, with the hose bend correction varying between 4 and 9 percent and sting bend correction varying between 4 and 6 percent.

Table 3. Typical Drag Corrections

Nominal Angle of Attack = +6 Degrees Re =  $5 \times 10^5$

Measured		C <sub>mu</sub>	Corrections		Correct C <sub>D</sub>
Alpha	C <sub>D</sub>		Hose	Sting Bend	
7.38	0.2974	0.1793	-0.0118	-0.0115	0.2741
7.37	0.2900	0.1742	-0.0118	-0.0114	0.2668
7.33	0.2773	0.1602	-0.0117	-0.0111	0.2545
7.32	0.2738	0.1522	-0.0117	-0.0110	0.2512
7.31	0.2643	0.1450	-0.0116	-0.0109	0.2418
7.27	0.2491	0.1323	-0.0116	-0.0105	0.2270
7.26	0.2417	0.1232	-0.0115	-0.0105	0.2197
7.24	0.2286	0.1164	-0.0115	-0.0103	0.2068
7.24	0.2348	0.1079	-0.0115	-0.0103	0.2130
7.21	0.2226	0.0987	-0.0114	-0.0100	0.2012
7.19	0.2172	0.0915	-0.0114	-0.0098	0.1960
7.18	0.2109	0.0824	-0.0114	-0.0098	0.1898
7.13	0.2040	0.0760	-0.0113	-0.0093	0.1834
7.14	0.1955	0.0678	-0.0113	-0.0094	0.1748
7.11	0.1918	0.0601	-0.0112	-0.0091	0.1714
7.06	0.1783	0.0524	-0.0111	-0.0087	0.1585
7.04	0.1699	0.0446	-0.0111	-0.0085	0.1503
7.02	0.1613	0.0371	-0.0110	-0.0084	0.1419
6.97	0.1432	0.0301	-0.0109	-0.0079	0.1243
6.93	0.1330	0.0225	-0.0109	-0.0076	0.1146
6.88	0.1162	0.0157	-0.0107	-0.0072	0.0983
6.72	0.0905	0.0000	-0.0104	-0.0058	0.0743

### **Equivalent Drag**

Equivalent drag is used to account for the fact that blowing air costs power. An aircraft utilizing a circulation control wing would have to provide the blowing air from engine power - most likely in the form of bleed air from the compressor section of a turbine engine. In order to compare blown wings with unblown wings, equivalent drag is defined as a measure of the energy cost of providing blowing air expressed as an additional drag term. Reference Englar (11).

$$D_e = D_{meas} + \frac{\Delta KE}{V_\infty \Delta t} + \dot{m} V_\infty \quad (25)$$

$$D_e = D_{meas} + \frac{\dot{m} V_j^2}{2 V_\infty} + \dot{m} V_\infty \quad (26)$$

or in coefficient form:

$$C_{De} = C_D + C_\mu \frac{V_j}{2 V_\infty} + C_\mu \frac{V_\infty}{V_j} \quad (27)$$

The free stream velocity was calculated from the Bernoulli equation and the ideal gas law.

$$q_\infty = \frac{\rho V_\infty^2}{2} \quad (28)$$

$$P_\infty = \rho_\infty R T_\infty = P_{atmos} - q_\infty \quad (29)$$

$$V_{\infty} = \left[ \frac{2q_{\infty} R T_{atmos}}{P_{atmos} - q_{\infty}} \right]^{1/2} \quad (30)$$

The second term in eq. 25 represents the power cost of providing the blowing air and the third term in eq. 25 represents an intake ram penalty.

#### Pitching Moment About the Leading Edge

The tunnel software reports pitching moment about the model center of gravity, so it was necessary to first transform the measured values of  $C_{Mcg}$  into measured values for  $C_{MLE}$ .  $C_{MLE}$  is more negative than  $C_{Mcg}$ .

$$C_{MLE} = C_{Mcg} - x_{cg} \frac{C_L}{C} \quad (31)$$

The location of the center of gravity is automatically determined by the tunnel software when tare slopes are computed. Only lift contributes to the pitching moment about the center of gravity because the force balance intersects the model center of gravity.

Pitching moment coefficient was not corrected for jet thrust. Pitching moment coefficient was corrected for hose attachment effects and sting bend in the same manner as the lift and drag coefficients. Equations of the form of eq. 22 were derived for  $C_{MLE}$  as a function of angle of attack and

corrections defined as for  $C_L$  and  $C_D$ . Typical corrections were less than 1 percent with both hose corrections and sting bend corrections less than 2 percent.

Table 4. Typical Moment Coefficient Corrections

Nominal Angle of Attack = +6 Degrees Re =  $5 \times 10^5$

Measured		Cmu	Corrections		Correct
Alpha	C <sub>MLE</sub>		Hose	Sting Band	C <sub>MLE</sub>
7.38	-0.7293	0.1793	0.0129	0.0109	-0.7055
7.37	-0.7199	0.1742	0.0129	0.0108	-0.6962
7.33	-0.6945	0.1602	0.0128	0.0105	-0.6712
7.32	-0.6834	0.1522	0.0128	0.0104	-0.6601
7.31	-0.6758	0.1450	0.0128	0.0104	-0.6527
7.27	-0.6488	0.1323	0.0128	0.0101	-0.6259
7.26	-0.6358	0.1232	0.0127	0.0100	-0.6131
7.24	-0.6196	0.1164	0.0127	0.0098	-0.5973
7.24	-0.6184	0.1079	0.0127	0.0098	-0.5958
7.21	-0.5939	0.0987	0.0127	0.0096	-0.5716
7.19	-0.5355	0.0915	0.0127	0.0094	-0.5634
7.18	-0.5723	0.0824	0.0126	0.0094	-0.5503
7.13	-0.5535	0.0760	0.0126	0.0090	-0.5319
7.14	-0.5395	0.0678	0.0126	0.0091	-0.5178
7.11	-0.5237	0.0601	0.0126	0.0088	-0.5023
7.06	-0.4899	0.0524	0.0125	0.0084	-0.4690
7.04	-0.4689	0.0446	0.0125	0.0083	-0.4482
7.02	-0.4425	0.0371	0.0124	0.0081	-0.4219
6.97	-0.4025	0.0301	0.0124	0.0077	-0.3824
6.93	-0.3755	0.0225	0.0123	0.0074	-0.3558
6.88	-0.3372	0.0157	0.0123	0.0070	-0.3179
6.72	-0.2384	0.0000	0.0121	0.0058	-0.2206



### Pressure Coefficient

Pressure data was taken for all data points during each run. Pressure coefficient is defined as:

$$C_p = \frac{P - P_\infty}{q_\infty} \quad (32)$$

Differential pressure referenced to atmospheric was recorded from the ESP modules. Tunnel total pressure was assumed to be atmospheric so pressure coefficient may be written as:

$$C_p = \frac{P - P_{atmos}}{q_\infty} + 1 \quad (33)$$

The surface pressure data contained many spurious data points, particularly at low blowing rates where the surface pressure values were small relative to the operating ranges of ESP modules. Obvious bad data points were disregarded. The remaining data points from the three spanwise locations of the model were averaged to show the general character of the chordwise pressure distribution between 6 and 10 inches inboard of the wingtip.

Section lift coefficients for the wing were calculated by numerical integration of the upper and lower surface pressures. These lift coefficients represent the section lift at a point eight in. inboard of the wingtip.

$$C_l = \left[ \frac{1}{c} \int_0^1 (C_{pl} - C_{pu}) dx \right] \cos \alpha \quad (34)$$

### **Pulsed Blowing**

Pulsed blowing presented the problem of correcting for nonconstant mass flow. Initially, data was presented in the form of the ratio of  $C_L$  to  $C_\mu$  versus pulsing frequency. Assuming that the slope of  $C_L$  versus  $C_\mu$  is fairly constant over small mass flow variations, this should allow frequency dependent trends to be readily seen. This scheme was less than successful by itself and was modified.

$C_L/C_\mu$  was plotted versus  $C_\mu$  and approximated by an equation of the form:

$$\frac{C_L}{C_\mu} = A(C_\mu)^k \quad (35)$$

where A and k are constants determined with the aid of a computer program (Grapher Copyright (C) 1988 Golden Software, Inc.) The result is plotted in Figure 16.

For each data point from the pulsed blowing runs, a point corresponding to steady state blowing with equivalent  $C_\mu$  was plotted for comparison.

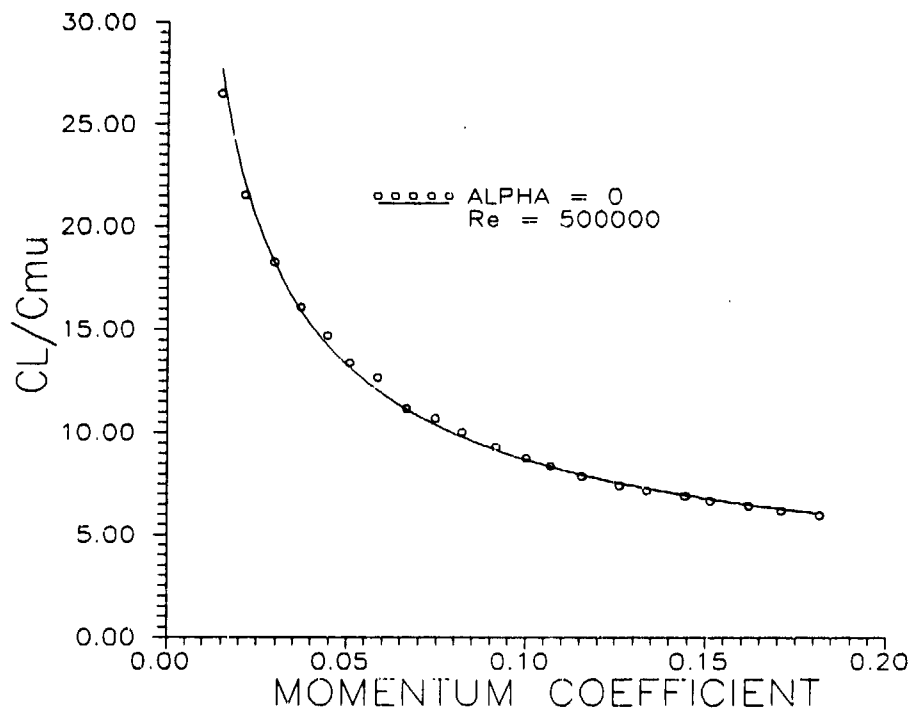


**Figure 16. Lift Coefficient to Momentum Coefficient Ratio  
versus Momentum Coefficient  $Re = 5 \times 10^5$**

## V. Results and Discussion

### Preliminary Testing

Initial testing found that the jet velocity was not completely uniform with the slot height set to 0.012 inches. Slot height was adjusted but complete uniformity was not possible. The final slot height varied, along the span, from 0.012 to 0.018 in. Before and after adjustment velocity profiles are presented in figures 7 and 8. The severe velocity dropoff at the left wing tip could not be rectified due to the slot height being fixed at the wing-tips. The low velocities away from the tips are at least partially due to the interference of the slot height adjustment posts.

Tuft studies showed that the jet remains strongly attached to the Coanda surface to approximately 135 degrees beyond vertical. Tufts also revealed strong vortices being shed from the wingtips. No spanwise flow was observed.

The pulser valve provides a sinusoidally modulated mass flow rate at low frequencies. At high frequencies, the mass flow modulation has the character of the absolute value of a sine wave. Flow is never completely cut off due to attenuation of the pulses because of compressibility of the air and flexibility of the hose. Flow rate oscillates about a mean value.

### **Primary Testing**

Lift coefficient versus momentum coefficient for angles of attack between -6 and 16 degrees are presented in Figure 17. Results show that the lift due to super-circulation has little dependence on angle of attack. Changes in angle of attack merely shift the  $C_L$  vs  $C_\mu$  curves up for increased angle of attack and down for decreased angle of attack. The results indicate there is a limit on circulation induced lift for three dimensional wings as theorized by McCormick (3). Deflection of the trailing vortex sheet is a second order effect that reduces lift by increasing downwash which reduces effective angle of attack. This effect is negligible for wings with high aspect ratios and no circulation augmentation, but has a significant effect on a circulation control wing with an aspect ratio of 2.325 such as the wing used in this study. Figure 18 presents experimental lift coefficient data from this study extrapolated out to momentum coefficients above 0.40. Logarithmic curve fitting was used.

$$C_L = 0.2924 \ln(C_\mu) + 2.217 \quad (36)$$

The extrapolated curve predicts a zero blowing  $C_L$  in good agreement with the measured value for 16 deg angle of attack. See Figure 11. The extrapolation to higher momentum coefficients is adequate to predict trends. The

theoretical limits (eq 5,6) proposed by McCormick (3) are also shown. From McCormick (1:59), the undeflected vortex sheet lift coefficient for a wing that generates circulation by angle of attack only is given by:

$$C_{l0} = \frac{2\pi\alpha}{1 + 2/AR} \quad (37)$$

and the lift slope is given by:

$$C_{l0_\alpha} = 1.075\pi \quad (38)$$

for  $AR = 2.325$ .

The measured lift slope without blowing was  $0.922\pi$ . Thus the deflected vortex sheet caused a 14 percent decrease in lift for the wing used in this study.

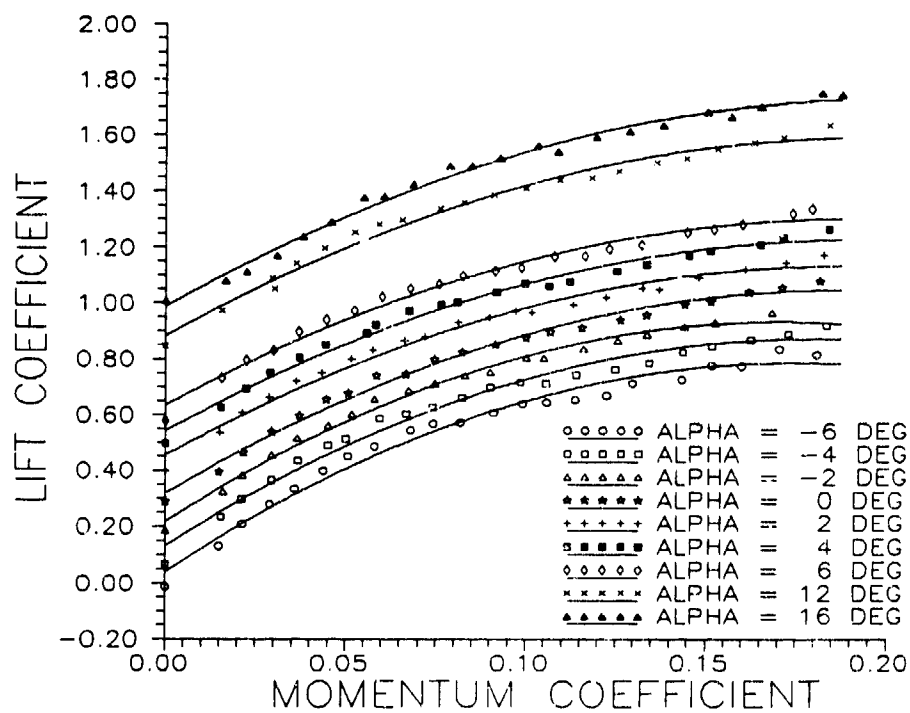


Figure 17. Lift Coefficient vs Momentum Coefficient  
 Effect of Blowing on Lift Coefficient  
 $Re = 5 \times 10^5$

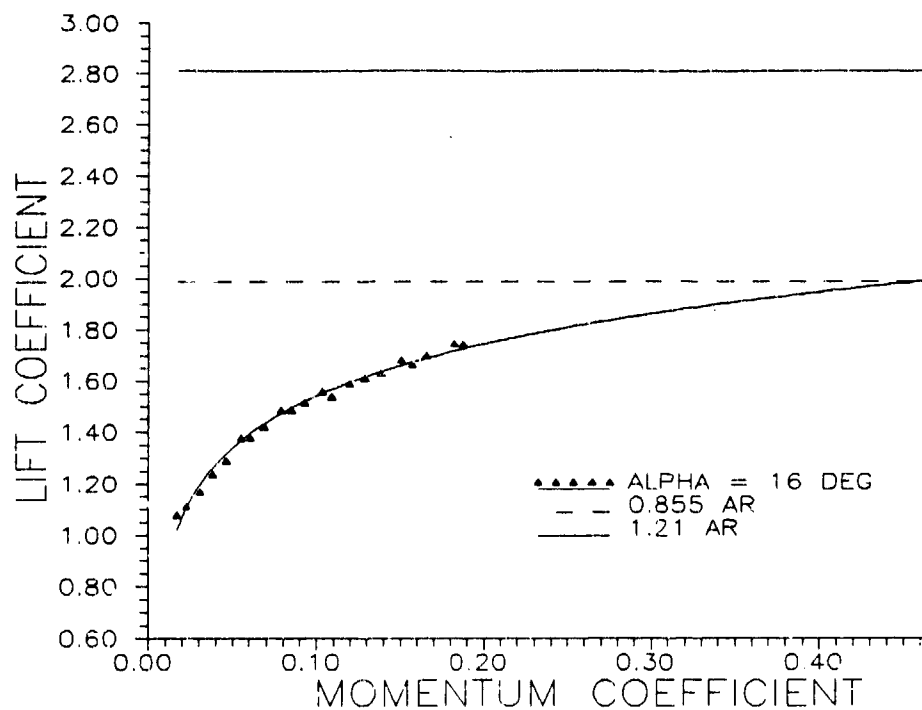


Figure 18. Lift Coefficient vs Momentum Coefficient  
Extrapolated to Higher Values of Momentum Coefficient.  $Re = 5 \times 10^5$  Limits Proposed by McCormick (3) Shown.



The flow trip installed on the Coanda surface had a detrimental effect on lift at 0 and +6 degrees angle of attack, but negligible effect at +16 degrees angle of attack. This indicates that for 0 and +6 degrees angle of attack, the jet was still attached at the location of the trip and that the trip caused separation and circulation was decreased. Comparison of lift coefficients with and without the flow trip installed are presented in Figure 19.

The flow trip significantly decreased drag for all three cases. This was expected for 0 and +6 degrees angle of attack because of the loss of lift due to the flow trip. The decrease in drag seemed to follow;

$$\Delta C_D = \frac{\Delta(C_L^2)}{\pi AR} \quad (39)$$

Which indicates that the decrease in drag was the result of lower induced drag due to decreased lift. The decrease in drag without degradation of lift at +16 degrees angle of attack indicates that there was a large suction peak on the Coanda surface that contributed more to drag than to lift. This is confirmed by the pressure coefficient plots. (See Figures 27 and 28)

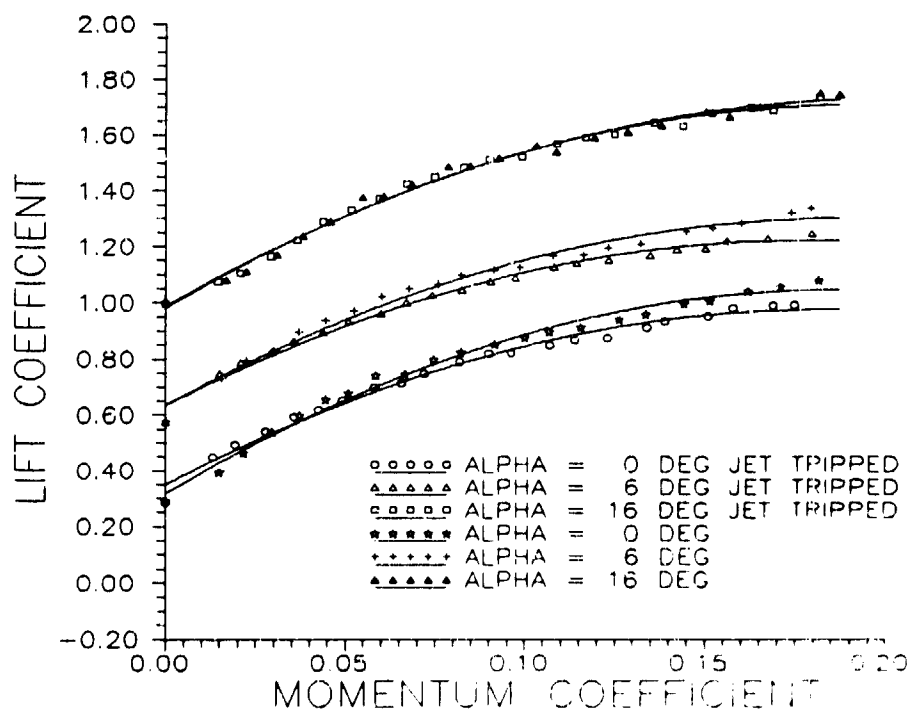


Figure 19. Lift Coefficient vs Momentum Coefficient -  
Comparison of Tripped and Untripped Jet  
 $Re = 5 \times 10^5$

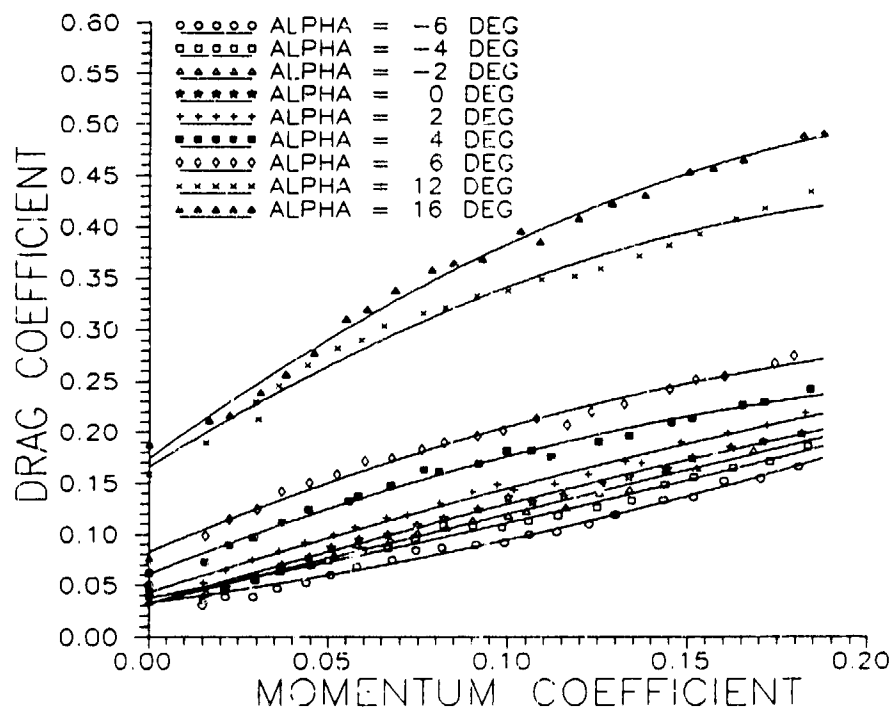


Figure 20. Corrected Drag Coefficient vs Momentum Coefficient  $Re = 5 \times 10^5$

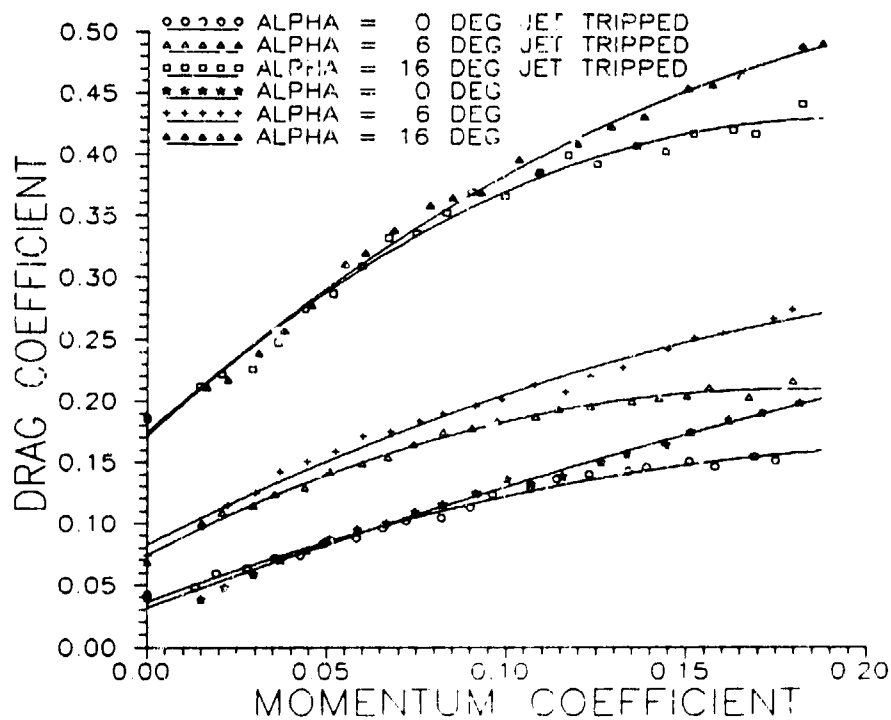
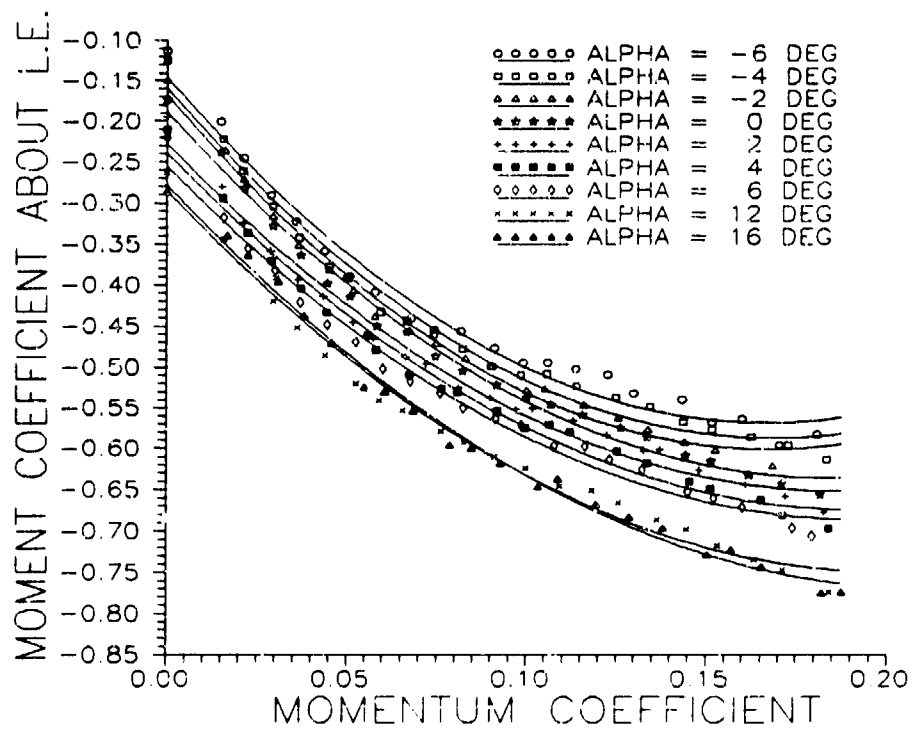


Figure 21. Corrected Drag Coefficient vs Momentum Coefficient - Comparison of Tripped and Untripped Jet  
 $Re = 5 \times 10^5$

Figure 22 shows that circulation control wings have large nose down pitching moments. This is due to the suction peak near the trailing edge. Figure 23 shows that tripping the jet at +16 deg angle of attack does not affect pitching moment coefficient. It seems likely that there is a suction peak localized on the vertical surface of the trailing edge that only affects drag. The difference in pitching moment coefficient with and without the trip installed at 0 and +6 deg angle of attack is due to the trip decreasing lift.



**Figure 22. Moment Coefficient About the Leading Edge vs  
Momentum Coefficient  $Re = 5 \times 10^5$**

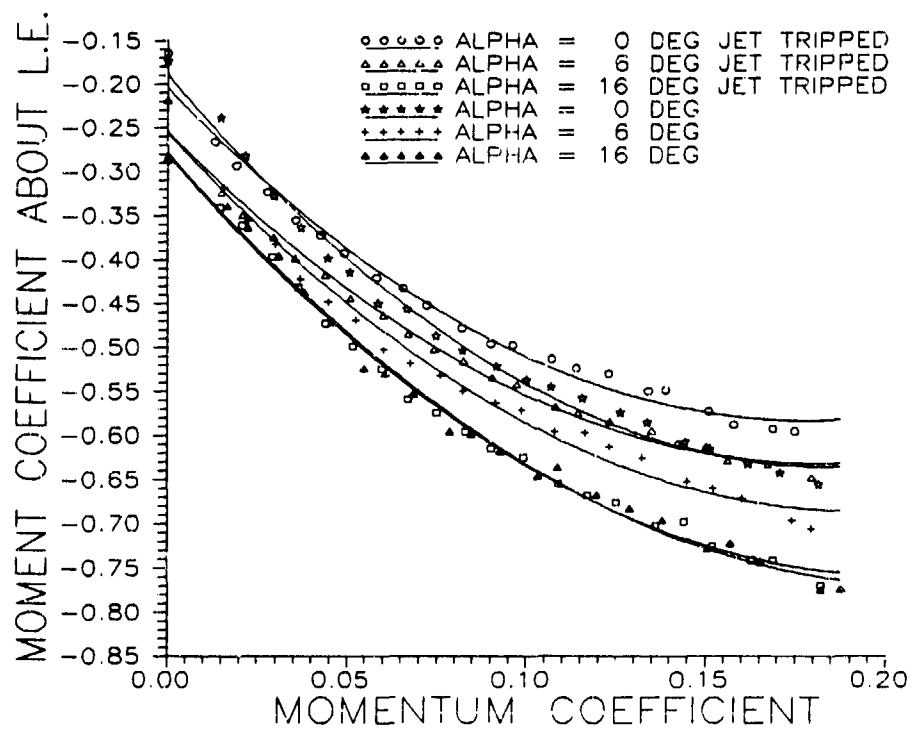


Figure 23. Moment Coefficient About the Leading Edge vs Momentum Coefficient - Comparison of Tripped and Untripped Jet

Pressure coefficient data was typical of a circulation control wing. Figure 24 shows the wing at 0.34 deg angle of attack with no blowing. Pressure coefficient data was not corrected for sting bend and the actual geometric angle of attack is shown in all  $C_p$  plots. As expected the forward stagnation point is located on the leading edge and there is a suction peak on the lower surface where the circular arc leading edge meets the flat bottom and there is a discontinuity in the slope. Figure 25 shows that even at 1.08 deg angle of attack, blowing creates a tremendous suction peak near the trailing edge of a circulation control wing. Figure 26 shows how increasing the angle of attack moves the forward stagnation point aft and significantly increases the pressure over the entire bottom of the wing. Figures 27 and 28 show how tripping the jet can decrease the suction peak on the trailing edge without greatly affecting the rest of the flow. Both  $C_p$  plots are for angle of attack near +18 deg and  $C_\mu = 0.1820$ . Figure 28 is for a run with the flow trip installed and has a significantly smaller suction peak at the trailing edge than in Figure 27 which is from a run without the flow trip installed. This indicates that in some cases additional circulation increases drag without a noticeable increase in lift.



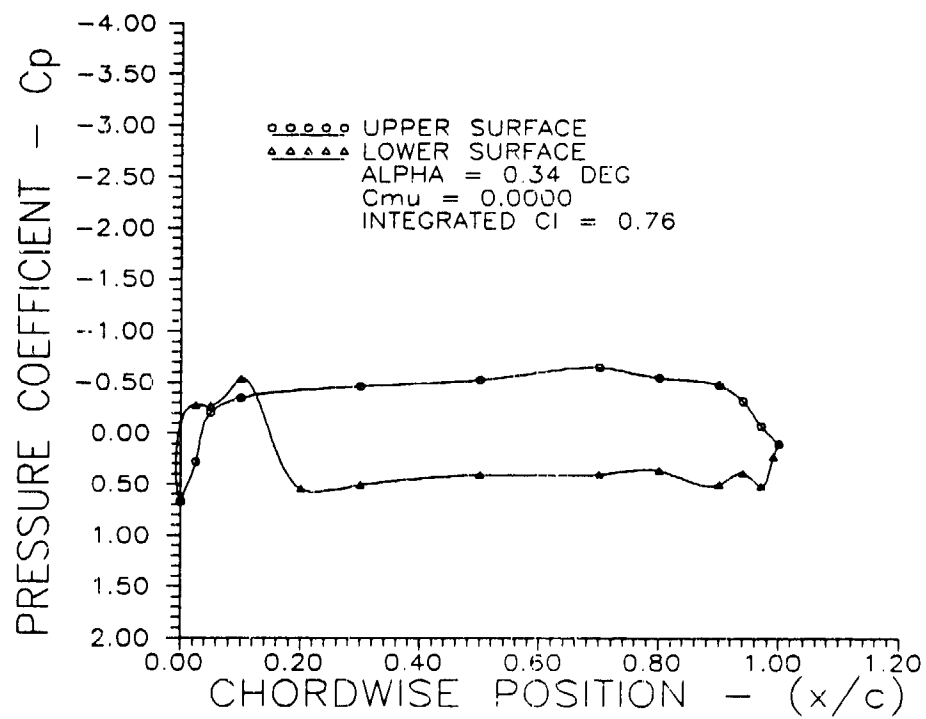


Figure 24. Pressure Coefficient vs Chordwise Position  
 $Re = 5 \times 10^5$

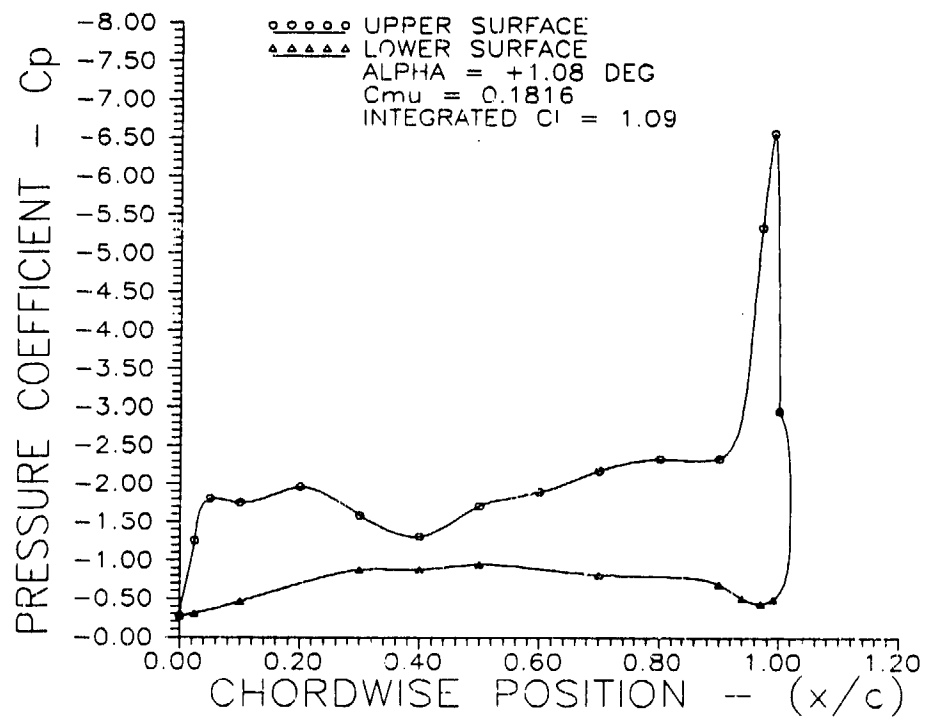


Figure 25. Pressure Coefficient vs Chordwise Position

Re =  $5 \times 10^5$

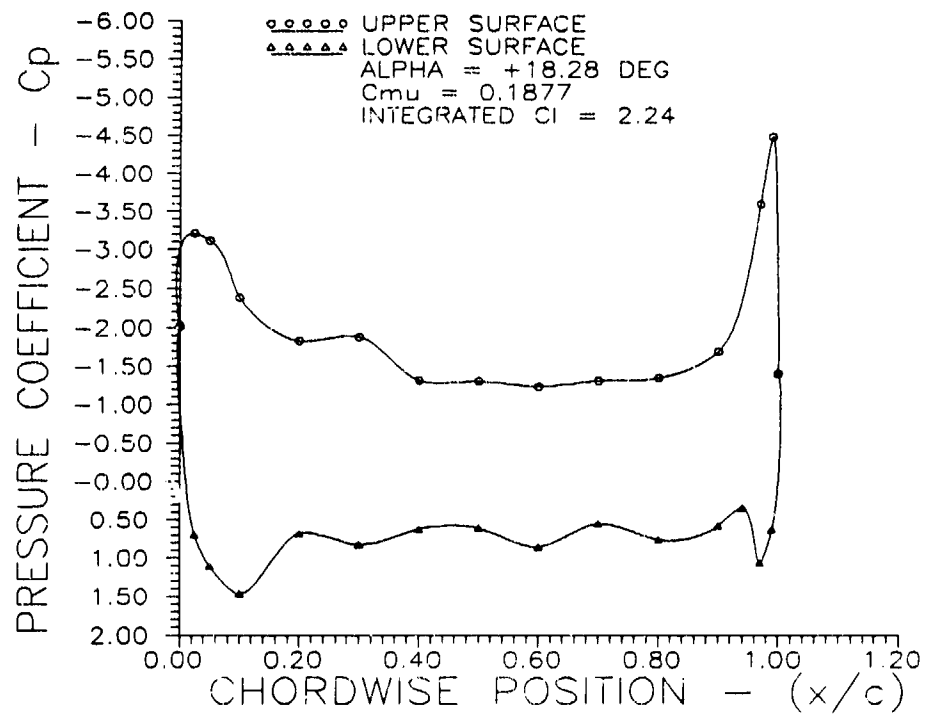


Figure 26. Pressure Coefficient vs Chordwise Position

Re =  $5 \times 10^5$

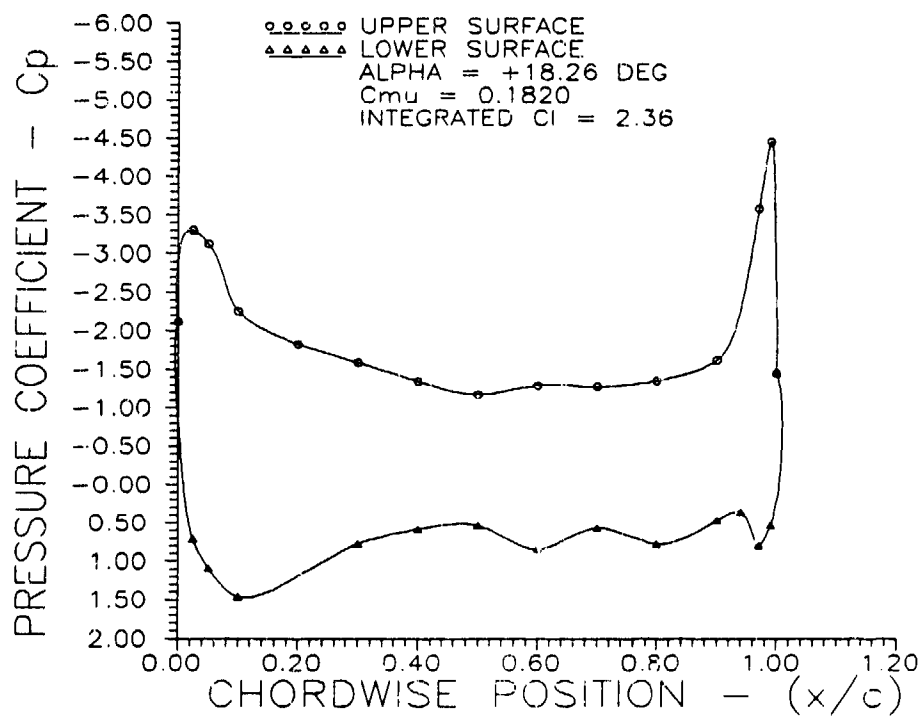
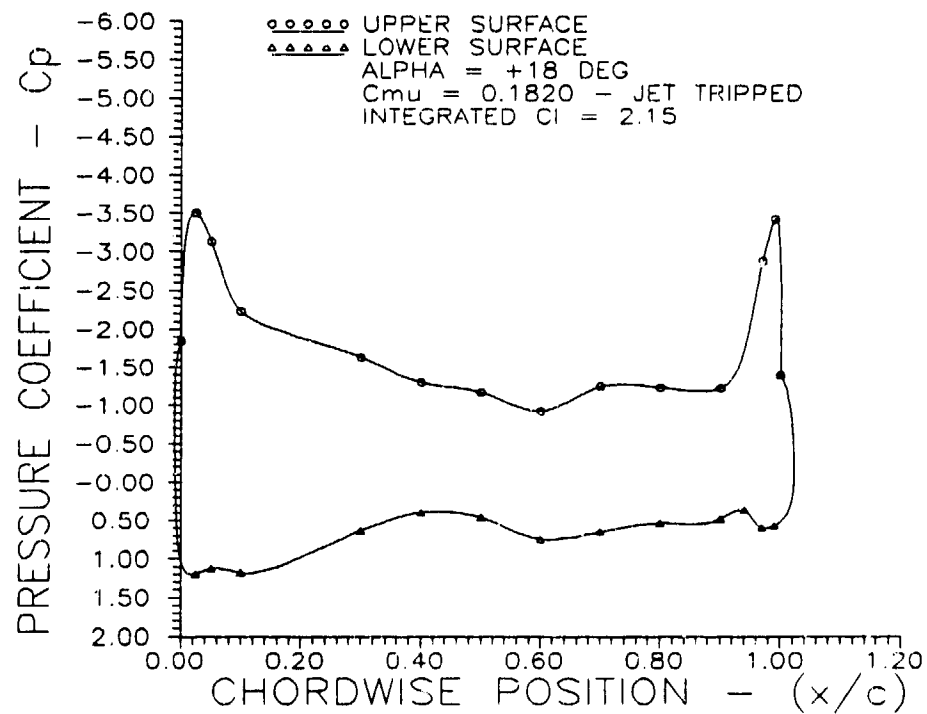


Figure 27. Pressure Coefficient vs Chordwise Position

Re = 5X10<sup>5</sup>



**Figure 28. Pressure Coefficient vs Chordwise Position**

**Re =  $5 \times 10^5$  - Jet Tripped**

Section lift coefficients, calculated from pressure data, were generally greater than the three dimensional lift coefficients measured by the force balance. Measured and calculated lift coefficients are compared in Table 5. Lift coefficients were smaller near the wingtips due to the non-elliptic planform of the wing model. Calculated  $C_L$  for +1.08 deg angle of attack at  $C_p = 0.1816$  was less than the measured  $C_L$ . This was likely due to the decrease of suction located on the upper surface at 0.40 chord. The low suction area may have been localized near the static pressure ports.

Table 5. Comparison of Measured Lift Coefficients with Section Lift coefficients Calculated from Surface Pressure Measurements

ANGLE OF ATTACK deg	MOMENTUM COEFFICIENT	MEASURED $C_L$	CALCULATED $C_L$
0.34	0.0000	0.30	0.76
1.08	0.1816	1.16	1.09
18.28	0.1877	1.85	2.24
18.26	0.1820	1.85	2.36
*18.29	0.1820	1.84	2.15

\* Jet tripped.

Figure 29 shows the lift to equivalent drag ratio versus lift coefficient. Lift to equivalent drag is useful for comparing circulation control wings to conventional wings in terms of power requirements for an aircraft using the wing. It is not meant to be used to predict the most efficient operating range of a circulation control wing as a traditional lift to drag plot is used with conventional wings.

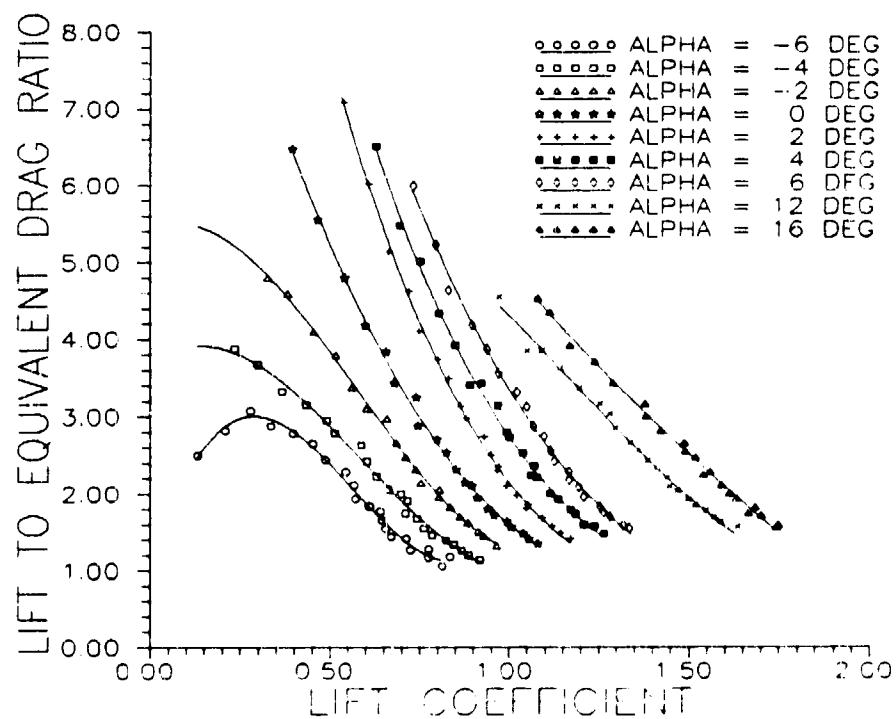


Figure 29. Lift to Equivalent Drag Ratio vs Lift Coefficient  $Re = 5 \times 10^5$

It was hoped to show greater lift augmentation for a given mass flow using pulsed blowing. Walters et al. (4)



demonstrated increased lift coefficients for a two dimensional cambered elliptical airfoil with blowing pulsed at or below 50 Hz.

In the present study pulsed blowing runs were made at low medium and high blowing coefficients. Measured lift coefficients were time averaged values. In all cases, pulsed blowing lift coefficients were less than steady state lift coefficients for a given momentum coefficient. Pulsed blowing lift coefficients came closest to matching the steady blowing lift coefficients at frequencies between 15 and 25 Hz.

Even at moderate momentum coefficients, pulsed blowing can be quite violent. The modulation of lift caused significant vibration of the model. The model shook violently when pulsed at frequencies near the resonant frequency of the sting balance/wing combination. The model suffered a structural failure during the last pulsed blowing run. The epoxy used to seal the plenum chambers failed and the lower skin separated from the leading edge allowing plenum pressure to vent through the seam. A review of pressure data confirmed that the failure occurred during the final run.

Data from the pulsed blowing runs is adequate for predicting trends, however detailed analysis is impossible due to the unknown effects of vibration on the sting balance.

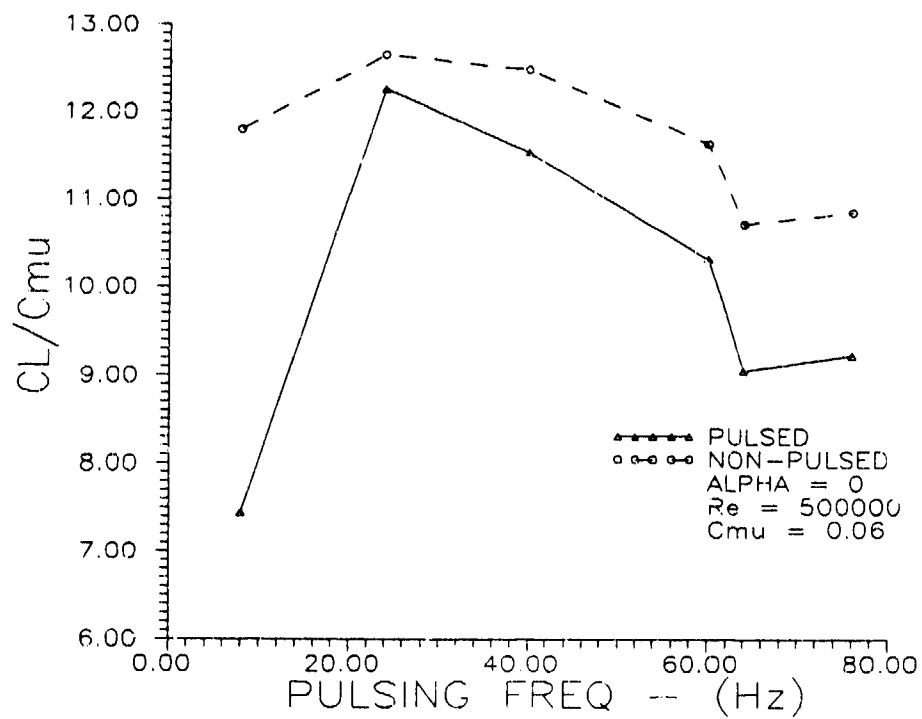


Figure 30. Lift Coefficient to Momentum Coefficient Ratio  
vs Pulsing Frequency - Low Momentum Coefficient  
 $Re = 5 \times 10^5$

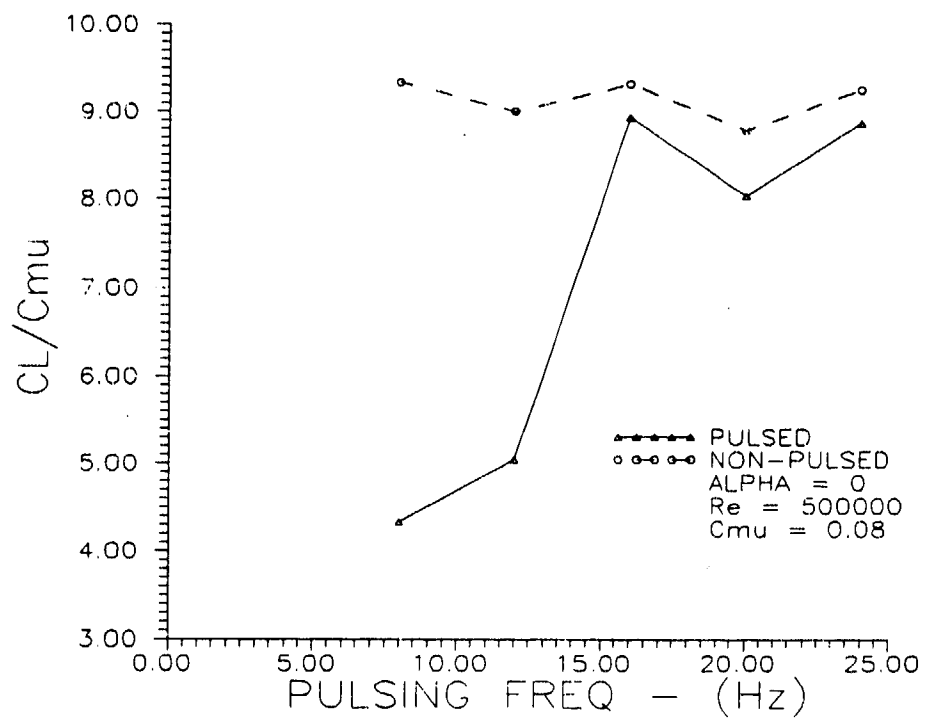


Figure 31. Lift Coefficient to Momentum Coefficient Ratio vs Pulsing Frequency - Medium Momentum Coefficient  $Re = 5 \times 10^5$

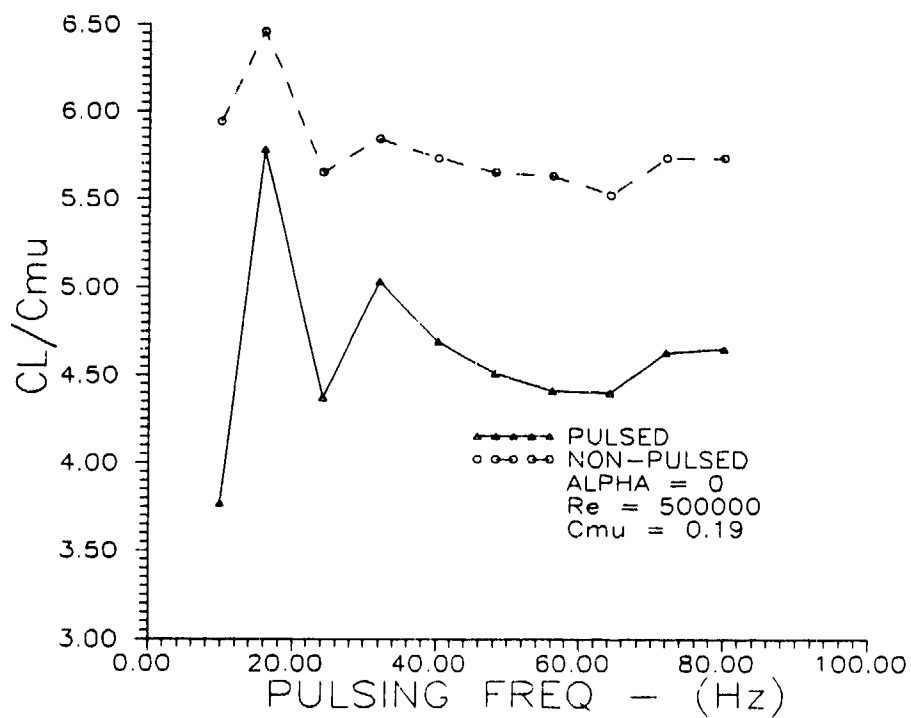


Figure 32. Lift Coefficient to Momentum Coefficient Ratio  
vs Pulsing Frequency - High Momentum Coefficient  
Re =  $5 \times 10^5$

## VI. Conclusions

1. There is a limit on maximum lift of a circulation control wing. Lift coefficients asymptotically approach this limit as momentum coefficient is increased. The results of this study support McCormick's (3) theory that this limit is due to deflection of the trailing vortex sheet and is determined by aspect ratio. Deflection of the trailing vortex sheet increases downwash such that beyond a certain point an increase in circulation will not result in higher lift. This does not contradict Kutta-Joukowski, but requires that the force vector be rotated back and the increase in its magnitude results in an increase in the drag component of the force only.
2. The trailing edge suction peak contributes significantly to drag and tripping the Coanda jet can, in some cases, decrease drag without degrading lift. The suction peak contributes to lift at angles of attack up to the point where it moves completely off the upper surface and onto the vertical portion of the trailing edge. In this study, the suction peak had moved off the wing upper surface at approximately +18 deg angle of attack.
3. Pulsing the jet could not be shown to increase lift per blowing mass flow. Pulsing the jet was shown to cause significant vibration that complicates sting-mounted wind

tunnel tests. Previous unsteady tests have been done with 2-dimensional models that can be mounted more securely at the walls of the tunnel. An extremely stiff sting balance is required to hold the model steady when using pulsed blowing. Oscillation of the model makes it very difficult to separate blowing effects from angle of attack effects.

4. The violent vibration caused by pulsed blowing could cause extreme problems if this technique were applied to conventional fixed wing aircraft. The vibration would likely be detrimental to both airframe structures and on board systems. Pulsing could be used for helicopter rotors as an alternative to physically changing the angle of attack as the rotor moves from the advancing side to the retreating side of the aircraft.

5. Interference effects of the Blowing hose/tube and the pressure port tubes were not significant. This method of testing circulation control wings is adequate.

#### VII. Recommendations

1. Further testing should be done with a new model. The new model should maintain the same span, but have an aspect ratio of 4 to 6. The new model tested with higher momentum coefficients could determine if a circulation control wing of moderate aspect ratio can develop more lift than wings with conventional mechanical high lift devices. The new

model should have an improved slot design that is stiffer to prevent bowing under pressure and a better means of slot height adjustment is needed.

2. Testing should go to higher blowing rates and determine the limit on lift of a higher aspect ratio wing. Results should be correlated with McCormick's theory (3).

3. Further investigation of tripping the Coanda jet to reduce drag should be done. A moveable trip should be used to determine the optimum separation point of the jet for maximum lift to drag at various angles of attack.

4. Pulsing should be studied further with a more robust model. A smaller planform would decrease forces and reduce the vibration problems. Experiments should be conducted with some of the blowing air bypassed around the pulser and the effects of different bypass ratios investigated.



### References

1. Kuethe, A.M. and Chow, C-Y, Foundations of Aerodynamics. New York: John Wiley and Sons, Inc., 1976
2. Ghee, T.A. and Leishman, J.G. Unsteady Circulation Control Aerodynamics of a Circular Cylinder with Periodic Jet Blowing, AIAA Paper 91-0433. University of Maryland, College Park, MD.
3. McCormick, B.W. Jr., Aerodynamics of V/STOL Flight. Orlando, FL: Academic Press Inc., 1967.
4. Walters, R.E., Myer, D.P., Holt, D.J., Circulation Control by Steady and Pulsed Blowing for a Cambered Elliptical Airfoil. NTIS AD-751 045. Arlington, VA: Office of Naval Research, July, 1972
5. Grumman Aerospace Corporation. Design of an A-6A Flight Demonstrator Aircraft Modified with a Circulation Control Wing (CCW). NSRDC Report CCW/1255-RE-01. Bethesda, MD: Naval Ship Research and Development Center, January 1978.

6. Harvell, Captain John K. An Experimental/Analytical Investigation into the Performance of a 20-Percent Thick, 8.5 Percent Cambered Circulation Controlled Airfoil. MS Thesis, AFIT/GAE/AA/82D-13. School of Engineering, Air Force Institute of Technology (AU), Wright-Patterson AFB OH, December 1982 (AD-124732).
7. Trainor, Captain John W. A Wind Tunnel Study of a Sting-Mounted Circulation Control Wing. MS Thesis, AFIT/GAE/ENY/89D-38. School of Engineering, Air Force Institute of Technology (AU), Wright-Patterson AFB OH, December 1989.
8. Pelletier, Captain Michael E. An Experimental Study of a Sting-mounted Single-Slot Circulation Control Wing. MS Thesis, AFIT/GAE/ENY/90D-18. School of Engineering, Air Force Institute of Technology (AU), Wright-Patterson AFB OH, December 1990.
9. Wood, N. And J. Nielson. Circulation Control Airfoils Past, Present, and Future. AIAA Paper 85-0204. American Institute of Aeronautics and Astronautics, January 1985.

10. Englar, R.J. Two-Dimensional Subsonic Wind Tunnel Tests of Two 15-Percent Thick Circulation Control Airfoils. NSRDC Technical Note AL-211. Bethesda, MD: Naval Ship Research and Development Center, August 1971.
11. Englar, R.J. Two-Dimensional Subsonic Wind Tunnel Investigations of a Cambered 30-Percent Thick Circulation Control Airfoil. NSRDC Technical Note AL-201. Bethesda, MD: Naval Ship Research and Development Center, May 1972
12. Pope, A. And W.H. Rae, Low Speed Wind Tunnel Testing. New York: John Wiley & Sons, Inc., 1984
13. Systems Research Laboratories. AFIT 5-ft Wind Tunnel Data Acquisition System. Version 1.3, User's Manual. Wright-Patterson AFB, OH, April 1990
14. Pressure Systems, Inc. Model 780B/T Pressure Measurement System User's Manual. First Edition, September 1983.

15. Doebelin, E.O. Measurement Systems Application and Design. New York: McGraw Hill, Inc., 1983

16. Trainor, J.W. and Franke, M.E. Wind Tunnel Study of a Sting-Mounted Circulation Control Wing. ISA Paper. School of Engineering, Air Force Institute of Technology (AU), Wright-Patterson AFB OH.

**Appendix 1**  
**Reduced Data**

Circ Control Wing  
 2:56:16pm on 9/26/91  
 Operator Capt. Lacher  
 Description Configuration clean wing  
 Comments No Problems  
 Barometric 28.9840

Pt	Alpha	Q	WindC <sub>L</sub>	WindC <sub>D</sub>	WindC <sub>M</sub>	Reynolds
1	-6.34	11.737	-0.0489	0.0413	-0.1226	5.0394E+05
2	-4.13	11.639	0.0616	0.0332	-0.0943	5.0097E+05
3	-1.81	11.741	0.2011	0.0303	-0.0598	5.0326E+05
4	0.33	11.731	0.3067	0.0336	-0.0305	5.0285E+05
5	2.42	11.680	0.4225	0.0415	0.0012	5.0176E+05
6	4.62	11.725	0.5103	0.0509	0.0334	5.0367E+05
7	6.78	11.735	0.6141	0.0681	0.0668	5.0423E+05
8	8.96	11.686	0.7041	0.0843	0.0970	5.0256E+05
9	11.19	11.719	0.8004	0.1090	0.1279	5.0351E+05
10	13.39	11.604	0.8999	0.1449	0.1569	5.0015E+05
11	15.57	11.498	0.9892	0.1733	0.1860	4.9882E+05
12	17.72	11.520	1.0444	0.1989	0.2107	5.0000E+05

Circ Control Wing  
 1:43:07pm on 9/27/91  
 Operator Capt. Lacher  
 Description Configuration w tube, hose -no blowing  
 Comments No Problems  
 Barometric 29.2650

Pt	Alpha	Q	WindC <sub>L</sub>	WindC <sub>D</sub>	WindC <sub>M</sub>	Reynolds
1	0.34	11.682	0.2980	0.0311	-0.0303	5.0776E+05
2	-6.30	11.551	-0.0704	0.0291	-0.1041	5.0390E+05
3	-4.11	11.556	0.0564	0.0304	-0.0812	5.0545E+05
4	-1.86	11.635	0.1820	0.0213	-0.0570	5.0700E+05
5	0.35	11.698	0.3100	0.0298	-0.0315	5.0709E+05
6	2.42	11.585	0.4159	0.0395	-0.0041	5.0540E+05
7	4.57	11.645	0.5254	0.0548	0.0226	5.0688E+05
8	6.73	11.613	0.6026	0.0758	0.0510	5.0519E+05
9	8.92	11.542	0.6940	0.1064	0.0776	5.0444E+05
10	11.15	11.570	0.7842	0.1306	0.1036	5.0475E+05
11	13.36	11.517	0.8753	0.1593	0.1265	5.0380E+05
12	15.53	11.413	0.9695	0.2002	0.1505	5.0201E+05
13	17.64	11.296	1.0360	0.2276	0.1741	5.0049E+05

Circulation Control Wing  
 Jet Thrust Run  
 Wind Off  
 12:40 pm 9/27/91  
 T = 67° P = 29.269 in Hg

pt	alpha deg	Axial Force lb <sub>f</sub>	Normal Force lb <sub>f</sub>	<i>m</i> slugs/sec
1	0.92	-1.0543	0.3913	0.004999
2	0.76	-0.9720	0.3202	0.004826
3	0.96	-0.8577	0.4130	0.004655
4	0.97	-0.9154	0.4270	0.004466
5	0.83	-0.9687	0.3550	0.004279
6	0.69	-0.9240	0.2792	0.004147
7	0.28	-0.9179	0.0848	0.003944
8	0.54	-0.8718	0.2157	0.003738
9	0.26	-0.8113	0.0843	0.003626
10	0.55	-0.7364	0.2336	0.003445
11	0.55	-0.7112	0.2273	0.003275
12	0.56	-0.5822	0.2339	0.003063
13	0.23	-0.4938	0.0735	0.002881
14	0.72	-0.4824	0.3209	0.002705
15	0.09	-0.3642	-0.0012	0.002529
16	0.22	-0.3034	0.0694	0.002345
17	0.29	-0.3133	0.1017	0.002157
18	0.09	-0.1997	-0.0005	0.001939
19	0.01	-0.1920	-0.0413	0.001723
20	-0.05	-0.0541	-0.0757	0.001500
21	-0.06	-0.0435	-0.0789	0.001282



Circ Control Wing  
 8:31:03am on 10/3/91  
 Operator Capt. Lacher  
 Description Configuration alpha = 16  
 Comments No Problems  
 Barometric 29.0140

$C_\mu$	$C_L$	$C_D$	$C_{MLE}$
0.1877	1.7435	0.4905	-0.7739
0.1820	1.7488	0.4387	-0.7743
0.1653	1.7004	0.4650	-0.7428
0.1570	1.6654	0.4569	-0.7221
0.1504	1.6835	0.4540	-0.7284
0.1381	1.6317	0.4308	-0.6961
0.1288	1.6115	0.4229	-0.6827
0.1195	1.5904	0.4084	-0.6673
0.1088	1.5397	0.3856	-0.6363
0.1033	1.5599	0.3959	-0.6458
0.0927	1.5176	0.3685	-0.6179
0.0848	1.4895	0.3645	-0.5991
0.0787	1.4870	0.3580	-0.5955
0.0686	1.4222	0.3381	-0.5531
0.0606	1.3808	0.3197	-0.5296
0.0549	1.3777	0.3105	-0.5241
0.0459	1.2900	0.2773	-0.4707
0.0381	1.2383	0.2568	-0.4370
0.0310	1.1690	0.2389	-0.3958
0.0225	1.1123	0.2172	-0.3637
0.0167	1.0799	0.2112	-0.3394
0.0000	1.0070	0.1876	-0.2868

Circ Control Wing  
 11:01:43am on 10/1/91  
 Operator Capt. Lacher  
 Description Configuration alpha = 12  
 Comments No Problems  
 Barometric 29.2630

$C_\mu$	$C_L$	$C_D$	$C_{MLE}$
0.1842	1.6342	0.4339	-0.7738
0.1714	1.5891	0.4173	-0.7464
0.1633	1.5707	0.4074	-0.7347
0.1532	1.5491	0.3928	-0.7172
0.1447	1.5157	0.3814	-0.6976
0.1363	1.4991	0.3708	-0.6866
0.1257	1.4677	0.3589	-0.6656
0.1184	1.4459	0.3518	-0.6509
0.1093	1.4390	0.3484	-0.6455
0.0999	1.4102	0.3376	-0.6239
0.0912	1.3855	0.3329	-0.6095
0.0826	1.3595	0.3214	-0.5928
0.0762	1.3382	0.3160	-0.5787
0.0656	1.2975	0.3038	-0.5532
0.0591	1.2811	0.2900	-0.5407
0.0525	1.2534	0.2823	-0.5204
0.0440	1.1960	0.2654	-0.4860
0.0363	1.1423	0.2455	-0.4519
0.0297	1.0901	0.2297	-0.4200
0.0304	1.0498	0.2126	-0.3920
0.0158	0.9720	0.1893	-0.3442
0.0000	0.8446	0.1583	-0.2630

Circ Control Wing  
 10:28:45am on 10/1/91  
 Operator Capt. Lacher  
 Description Configuration alpha = 6  
 Comments No Problems  
 Barometric 29.2640

$C_u$	$C_L$	$C_D$	$C_{MLE}$
0.1793	1.3350	0.2741	-0.7055
0.1742	1.3199	0.2668	-0.6962
0.1602	1.2816	0.2545	-0.6712
0.1522	1.2636	0.2512	-0.6601
0.1450	1.2520	0.2418	-0.6527
0.1323	1.2085	0.2270	-0.6259
0.1232	1.1939	0.2197	-0.6131
0.1164	1.1673	0.2068	-0.5973
0.1079	1.1659	0.2130	-0.5958
0.0987	1.1260	0.2012	-0.5716
0.0915	1.1152	0.1960	-0.5634
0.0824	1.0968	0.1898	-0.5503
0.0760	1.0665	0.1834	-0.5319
0.0678	1.0491	0.1748	-0.5178
0.0601	1.0219	0.1714	-0.5023
0.0524	0.9704	0.1585	-0.4690
0.0446	0.9374	0.1503	-0.4482
0.0371	0.8962	0.1419	-0.4219
0.0301	0.8303	0.1243	-0.3824
0.0225	0.7943	0.1146	-0.3558
0.0157	0.7322	0.0983	-0.3179
0.0000	0.5778	0.0743	-0.2206

Circ Control Wing  
 9:53:43am on 10/1/91  
 Operator Capt. Lacher  
 Description Configuration alpha = 4  
 Comments No Problems  
 Barometric 29.2610

$C_\mu$	$C_L$	$C_D$	$C_{MLE}$
0.1840	1.2643	0.2416	-0.6964
0.1713	1.2364	0.2296	-0.6803
0.1652	1.2084	0.2267	-0.6629
0.1512	1.1856	0.2131	-0.6486
0.1455	1.1721	0.2094	-0.6399
0.1336	1.1377	0.1962	-0.6178
0.1253	1.1140	0.1903	-0.6034
0.1121	1.0764	0.1760	-0.5791
0.1064	1.0605	0.1822	-0.5706
0.0996	1.0706	0.1818	-0.5744
0.0919	1.0374	0.1696	-0.5538
0.0809	1.0005	0.1614	-0.5307
0.0765	0.9925	0.1632	-0.5257
0.0675	0.9690	0.1477	-0.5092
0.0582	0.9209	0.1370	-0.4789
0.0558	0.8905	0.1325	-0.4609
0.0444	0.8495	0.1239	-0.4338
0.0372	0.8033	0.1120	-0.4043
0.0291	0.7509	0.0969	-0.3706
0.0223	0.6939	0.0893	-0.3366
0.0155	0.6274	0.0726	-0.2946
0.0000	0.4960	0.0616	-0.2110

Circ Control Wing  
 9:16:59am on 10/1/91  
 Operator Capt. Lacher  
 Description Configuration alpha = 2  
 Comments No Problems  
 Barometric 29.2660

$C_\mu$	$C_L$	$C_D$	$C_{MLE}$
0.1826	1.1724	0.2185	-0.6766
0.1721	1.1434	0.2066	-0.6580
0.1612	1.1199	0.1989	-0.6434
0.1481	1.0913	0.1897	-0.6263
0.1371	1.0473	0.1692	-0.6016
0.1326	1.0537	0.1711	-0.6027
0.1224	1.0205	0.1584	-0.5838
0.1132	0.9916	0.1494	-0.5659
0.1017	0.9660	0.1432	-0.5504
0.0972	0.9705	0.1484	-0.5517
0.0900	0.9486	0.1411	-0.5373
0.0811	0.9288	0.1305	-0.5254
0.0720	0.8787	0.1184	-0.4960
0.0663	0.8649	0.1163	-0.4869
0.0575	0.8309	0.1070	-0.4651
0.0517	0.8006	0.0995	-0.4457
0.0433	0.7493	0.0916	-0.4137
0.0363	0.7203	0.0832	-0.3942
0.0289	0.6625	0.0753	-0.3589
0.0213	0.6073	0.0649	-0.3240
0.0152	0.5362	0.0517	-0.2807
0.0000	0.3997	0.0432	-0.1950

Circ Control Wing  
 10:58:43am on 9/30/92  
 Operator Capt. Lacher  
 Description Configuration alpha = 0  
 Comments No Problems  
 Barometric 29.4440

$C_u$	$C_L$	$C_D$	$C_{MLE}$
0.1816	1.0796	0.1083	-0.6555
0.1710	1.0548	0.1905	-0.6423
0.1620	1.0383	0.1846	-0.6319
0.1514	1.0064	0.1745	-0.6150
0.1443	0.9946	0.1636	-0.6080
0.1337	0.9573	0.1563	-0.5859
0.1263	0.9388	0.1500	-0.5741
0.1157	0.9111	0.1385	-0.5578
0.1069	0.8955	0.1318	-0.5454
0.1001	0.8765	0.1360	-0.5369
0.0917	0.8525	0.1245	-0.5213
0.0823	0.8247	0.1154	-0.5036
0.0747	0.7980	0.1095	-0.4867
0.0667	0.7452	0.1001	-0.4566
0.0585	0.7402	0.0952	-0.4495
0.0508	0.6777	0.0871	-0.4141
0.0446	0.6552	0.0780	-0.3979
0.0372	0.5976	0.0700	-0.3635
0.0296	0.5400	0.0588	-0.3275
0.0216	0.4650	0.0481	-0.2821
0.0149	0.3947	0.0384	-0.2381
0.0000	0.2910	0.0401	-0.1733

Circ Control Wing  
 10:14:22am on 9/30/91  
 Operator Capt. Lacher  
 Description Configuration alpha = -2  
 Comments No Problems  
 Barometric 29.4530

$C_{\mu}$	$C_L$	$C_D$	$C_{MLE}$
0.1684	0.9646	0.1817	-0.6207
0.1526	0.9291	0.1643	-0.6018
0.1441	0.9150	0.1628	-0.5920
0.1339	0.8846	0.1432	-0.5763
0.1256	0.8636	0.1400	-0.5621
0.1162	0.8357	0.1261	-0.5455
0.1051	0.8018	0.1221	-0.5259
0.1002	0.8047	0.1182	-0.5276
0.0902	0.7534	0.1135	-0.4983
0.0830	0.7391	0.1064	-0.4885
0.0748	0.7106	0.1015	-0.4706
0.0675	0.6845	0.0947	-0.4553
0.0580	0.6574	0.0897	-0.4376
0.0518	0.6019	0.0798	-0.4060
0.0452	0.5603	0.0712	-0.3813
0.0366	0.5159	0.0643	-0.3512
0.0296	0.4539	0.0564	-0.3156
0.0214	0.3818	0.0476	-0.2714
0.0161	0.3254	0.0429	-0.2363
0.0000	0.1862	0.0342	-0.1486

Circ Control Wing  
 9:24:19am on 9/30/91  
 Operator Capt. Lacher  
 Description Configuration alpha = -4  
 Comments No Problems  
 Barometric 29.4680

$C_\mu$	$C_L$	$C_D$	$C_{MLE}$
0.1834	0.9184	0.1854	-0.6133
0.1729	0.8870	0.1709	-0.5959
0.1626	0.8684	0.1651	-0.5858
0.1517	0.8455	0.1557	-0.5771
0.1438	0.8232	0.1486	-0.5676
0.1345	0.7844	0.1326	-0.5485
0.1249	0.7623	0.1260	-0.5364
0.1141	0.7431	0.1181	-0.5226
0.1058	0.7113	0.1126	-0.5078
0.0985	0.7167	0.1068	-0.5089
0.0902	0.6978	0.1079	-0.4986
0.0823	0.6608	0.1089	-0.4775
0.0742	0.6281	0.0962	-0.4591
0.0668	0.6025	0.0868	-0.4438
0.0595	0.5865	0.0839	-0.4328
0.0501	0.5140	0.0741	-0.3917
0.0451	0.4895	0.0695	-0.3778
0.0367	0.4328	0.0639	-0.3428
0.0295	0.3656	0.0546	-0.3037
0.0211	0.2977	0.0455	-0.2609
0.0155	0.2341	0.0360	-0.2222
0	0.0689	0.0479	-0.1247



Circ Control Wing  
 2:20:55pm on 9/27/91  
 Operator Capt. Lacher  
 Description Configuration alpha = -6  
 Comments No Problems  
 Barometric 29.2580

$C_\mu$	$C_L$	$C_D$	$C_{MLE}$
0.1808	0.8133	0.1654	-0.5829
0.1704	0.8351	0.1540	-0.5963
0.1601	0.7735	0.1518	-0.5630
0.1517	0.7755	0.1360	-0.5678
0.1434	0.7248	0.1333	-0.5392
0.1299	0.7132	0.1191	-0.5315
0.1226	0.6698	0.1101	-0.5093
0.1138	0.6536	0.1024	-0.5021
0.1059	0.6450	0.1001	-0.4945
0.0991	0.6398	0.0920	-0.4945
0.0911	0.6085	0.0898	-0.4765
0.0818	0.5713	0.0864	-0.4562
0.0744	0.5670	0.0841	-0.4548
0.0680	0.5436	0.0749	-0.4404
0.0580	0.4863	0.0681	-0.4087
0.0507	0.4517	0.0598	-0.3897
0.0438	0.3976	0.0524	-0.3585
0.0359	0.3344	0.0467	-0.3231
0.0290	0.2789	0.0384	-0.2905
0.0213	0.2076	0.0387	-0.2457
0.0149	0.1315	0.0303	-0.2008
0.0000	-0.0138	0.0498	-0.1135

Circ Control Wing  
 9:54:00am on 10/7/91  
 Operator Capt. Lacher  
 Description Configuration jet tripped  
 ALPHA = 16  
 Comments No Problems  
 Barometric 29.3750

$C_\mu$	$C_L$	$C_D$	$C_{MLE}$
0.1820	1.7338	0.4411	-0.7694
0.1690	1.6881	0.4167	-0.7411
0.1630	1.6964	0.4203	-0.7411
0.1520	1.6775	0.4167	-0.7255
0.1440	1.6299	0.4022	-0.6979
0.1360	1.6421	0.4068	-0.7028
0.1250	1.6019	0.3916	-0.6761
0.1170	1.5908	0.3988	-0.6686
0.1090	1.5676	0.3846	-0.6543
0.0993	1.5231	0.3658	-0.6249
0.0902	1.5131	0.3692	-0.6152
0.0832	1.4832	0.3522	-0.5965
0.0750	1.4500	0.3357	-0.5744
0.0672	1.4253	0.3316	-0.5592
0.0596	1.3716	0.3089	-0.5247
0.0516	1.3317	0.2866	-0.4992
0.0440	1.2880	0.2739	-0.4728
0.0366	1.2229	0.2475	-0.4319
0.0293	1.1640	0.2255	-0.3971
0.0207	1.1052	0.2217	-0.3616
0.0147	1.0780	0.2118	-0.3411
0.0000	0.9949	0.1855	-0.2867

Circ Control Wing  
 10:30:34am on 10/7/91  
 Operator Capt. Lacher  
 Description Configuration alpha=6 jet tripped  
 Comments No Problems  
 Barometric 29.3730

$C_\mu$	$C_L$	$C_D$	$C_{MLE}$
0.1797	1.2456	0.2160	-0.6477
0.1675	1.2272	0.2031	-0.6332
0.1563	1.2205	0.2104	-0.6289
0.1503	1.1905	0.2040	-0.6127
0.1424	1.1882	0.2019	-0.6089
0.1349	1.1662	0.1997	-0.5954
0.1234	1.1512	0.1950	-0.5843
0.1145	1.1392	0.1930	-0.5749
0.1082	1.1271	0.1868	-0.5681
0.0974	1.0879	0.1834	-0.5426
0.0905	1.0766	0.1779	-0.5345
0.0826	1.0458	0.1744	-0.5157
0.0743	1.0272	0.1644	-0.5024
0.0671	1.0013	0.1538	-0.4853
0.0600	0.9627	0.1486	-0.4637
0.0509	0.9347	0.1422	-0.4441
0.0440	0.8933	0.1289	-0.4176
0.0357	0.8636	0.1239	-0.3989
0.0295	0.8252	0.1141	-0.3745
0.0209	0.7870	0.1085	-0.3495
0.0152	0.7472	0.1001	-0.3235
0.0000	0.5746	0.0684	-0.2185

Circ Control Wing  
 9:14:59am on 10/7/91  
 Operator Capt. Lacher  
 Description Configuration flow trip on  
 ALPHA = 0  
 Comments No Problems  
 Barometric 29.3670

$C_\mu$	$C_L$	$C_D$	$C_{MLE}$
0.1750	0.9900	0.1510	-0.5957
0.1690	0.9886	0.1542	-0.5927
0.1580	0.9794	0.1459	-0.5887
0.1510	0.9491	0.1503	-0.5736
0.1390	0.9319	0.1456	-0.5492
0.1340	0.9103	0.1424	-0.5501
0.1230	0.8733	0.1397	-0.5300
0.1140	0.8663	0.1362	-0.5243
0.1070	0.8490	0.1285	-0.5137
0.0962	0.8217	0.1234	-0.4980
0.0901	0.8215	0.1132	-0.4962
0.0820	0.7916	0.1042	-0.4784
0.0721	0.7483	0.1018	-0.4522
0.0657	0.7141	0.0960	-0.4323
0.0582	0.6983	0.0878	-0.4210
0.0492	0.6512	0.0837	-0.3927
0.0426	0.6179	0.0736	-0.3723
0.0357	0.5931	0.0717	-0.3551
0.0278	0.5411	0.0636	-0.3231
0.0192	0.4927	0.0593	-0.2931
0.0133	0.4495	0.0482	-0.2657
0.0000	0.2857	0.0421	-0.1647

HIGH BLOWING COEFF  
 Circ Control Wing  
 9:38:34am on 10/3/91  
 Operator Capt. Lacher  
 Description Configuration alpha=0,pulsed  
 Comments shut down because grease in hose  
 Barometric 29.0250

Freq (Hz)	$C_u$	$C_L$	$C_D$	$C_{MLE}$
9.88	0.187	0.7053	0.1810	-0.4034
16.00	0.163	0.9422	0.1716	-0.5648
24.16	0.203	0.8875	0.1677	-0.5461
32.00	0.192	0.9659	0.1467	-0.5852
40.20	0.198	0.9290	0.1519	-0.5633
48.20	0.203	0.9157	0.1539	-0.5518
56.16	0.204	0.8988	0.1370	-0.5446
64.24	0.211	0.9285	0.1371	-0.5607
72.00	0.198	0.9166	0.1379	-0.5571
80.00	0.198	0.9209	0.1424	-0.5595

Circ Control Wing  
 10:33:08am on 10/9/91  
 Operator Capt. Lacher  
 Description Configuration alpha=0 pulsed  
 MED BLOWING  
 Comments No Problems  
 Barometric 29.3110

freq (Hz)	$C_\mu$	$C_L$	$C_D$	$C_{MLE}$
8	0.0889	0.3853	0.0487	-0.2496
12	0.0945	0.4768	0.1127	-0.3061
16	0.0893	0.7972	0.0968	-0.4788
20	0.0984	0.7897	0.1065	-0.4760
24	0.0904	0.8014	0.0955	-0.4818
20	0.0946	0.7914	0.1043	-0.4756
16	0.0852	0.8401	0.1142	-0.4990
12	0.1206	1.1273	0.0841	-0.6487
8	0.0360	1.0981	0.1397	-0.6543

LOW BLOWING COEFF  
 Circ Control Wing  
 11:09:19am on 10/3/91  
 Operator Capt. Lacher  
 Description Configuration alpha=0 pulsed  
 Comments No Problems  
 Barometric 29.0460

Freq (Hz)	$C_\mu$	$C_L$	$C_D$	$C_{MLE}$
8.00	0.0606	0.4508	0.0680	-0.2514
24.00	0.0541	0.5635	0.0563	-0.3957
40.00	0.0553	0.6377	0.0660	-0.3833
60.00	0.0621	0.6402	0.0666	-0.3852
64.00	0.0711	0.6431	0.0603	-0.3877
76.00	0.0697	0.6423	0.0619	-0.3876

Pressure Coefficient data:

Angle of attack = 0.34;  $C_{\mu} = 0$ ;  $Re = 507000$

X/C	$C_p$ upper	$C_p$ lower
0.0000	0.6664	0.6664
0.0250	0.2836	-0.2753
0.0500	-0.2027	-0.2691
0.1000	-0.3479	-0.5350
0.2000	----	0.5495
0.3000	-0.4624	0.5076
0.4000	----	----
0.5000	-0.5264	0.4054
0.6000	----	----
0.7000	-0.6495	0.4017
0.8000	-0.5486	0.3636
0.9000	-0.4747	0.5002
0.9400	-0.3196	0.3894
0.9700	-0.0734	0.5138
0.9900	----	0.2269
1.0000	0.1002	0.1002



Pressure Coefficient data:

Angle of attack = 1.08;  $C_\mu = 0.1816$ ;  $Re = 492640$

X/C	$C_p$ upper	$C_p$ lower
0.0000	-0.2695	-0.2695
0.0250	-1.2559	-0.3069
0.0500	-1.8013	----
0.1000	-0.5970	-0.4629
0.2000	-1.9573	----
0.3000	-1.5872	-0.8755
0.4000	-1.3126	-0.8832
0.5000	-1.7110	-0.9490
0.6000	-1.8954	----
0.7000	-2.1752	-0.8110
0.8000	-2.3287	----
0.9000	-2.3377	-0.6911
0.9400	0.7504	-0.5093
0.9700	-5.3368	-0.4397
0.9900	-6.5605	-0.4977
1.0000	-2.9553	-2.9553

Pressure Coefficient data

Angle of attack = 18.28;  $C_\mu = .1877$ ;  $Re = 477130$

X/C	$C_p$ upper	$C_p$ lower
0.0000	-2.0249	-2.0249
0.0250	-3.2095	0.7025
0.0500	-3.1153	1.1023
0.1000	-2.3870	1.4631
0.2000	-1.8310	0.6823
0.3000	-1.8822	0.8263
0.4000	-1.3181	0.6217
0.5000	-1.3073	0.6096
0.6000	-1.2387	0.8573
0.7000	-1.3127	0.5544
0.8000	-1.3477	0.7617
0.9000	-1.6950	0.5840
0.9400	1.7175	0.3485
0.9700	-3.5972	1.0713
0.9900	-4.4857	0.6271
1.0000	-1.4097	-1.4097

Pressure Coefficient data

Angle of attack = 18.26;  $C_{\mu}$  = .1820; Re = 491640

Jet Tripped

---

x/c	$C_p$ upper	$C_p$ lower
-----	-------------	-------------

---

0.0000	-1.8532	-1.8532
0.0250	-3.5045	1.1922
0.0500	-3.1296	1.1245
0.1000	-2.2322	1.1773
0.2000	----	----
0.3000	-1.6312	0.6318
0.4000	-1.3023	0.3923
0.5000	-1.1670	0.4613
0.6000	-0.9193	0.7415
0.7000	-1.2482	0.6454
0.8000	-1.2306	0.5371
0.9000	-1.2198	0.4816
0.9400	----	0.3652
0.9700	-2.8737	0.5939
0.9900	-3.4179	0.5696
1.0000	-1.3971	-1.3971

Pressure Coefficient Data

Alpha = 18.29;  $C_\mu$  = .1820; Re = 477820

x/c	C <sub>p</sub> upper	C <sub>p</sub> lower
0.0000	-2.1211	-2.1211
0.0250	-3.2971	0.7131
0.0500	-3.1233	1.0916
0.1000	-2.2504	1.4634
0.2000	-1.8288	----
0.3000	-1.5850	0.7764
0.4000	-1.3425	0.5838
0.5000	-1.1728	0.5339
0.6000	-1.2886	0.8464
0.7000	-1.2738	0.5649
0.8000	-1.3506	0.7777
0.9000	-1.6187	0.4733
0.9400	----	0.3628
0.9700	-3.5800	0.7979
0.9900	-4.4556	0.5326
1.0000	-1.4449	-1.4449

## **Appendix 2**

### **Data Accuracy**

#### **Force Balance and Wind Tunnel Data**

Force balance and wind tunnel raw data were acquired through the wind tunnel software to 10 significant figures. During data reduction and retrieval the data was rounded to 4 decimal places. This data was reduced to aerodynamic coefficients.

#### **Surface Pressure Data**

Surface pressure data was recorded from the 780B/T pressure measurement system to 4 decimal places. Accuracy of the pressure measurement system is 0.10 percent of full scale (14). Therefore, accuracy of the suction surface data was 0.005 psid and accuracy of the pressure surface and plenum was 0.045 psid.

#### **Atmospheric Data**

Atmospheric temperature was recorded by hand from a mercury thermometer to the nearest half degree Fahrenheit. Atmospheric pressure was recorded from a mercury manometer to the nearest thousandth of an inch of mercury and corrected for temperature and instrument error.

#### **Secondary Air Data**

Venturi pressures were recorded from pressure transducers accurate to 0.01 psid using digital multimeters

accurate to 0.0005 Volt. Venturi and plenum temperatures were recorded using thermocouples accurate to 0.05 degree Fahrenheit.

**Overall Accuracy**

Overall accuracy is to within 2 percent except for the pulsed blowing runs that are estimated to be within 7 percent.

### Vita

Captain Steven J. Lacher was born on 21 September 1963 in Columbus, Ohio. He graduated from Walnut Ridge High School in Columbus in 1981. In 1985 he graduated from Boston University with a Bachelor of Science degree in Aerospace Engineering and was commissioned through the Reserve Officer Training Corps program. From October of 1985 until April 1990 he served as an A-10A and F-111 aircraft structural engineer at Sacramento Air Logistics Center, McClellan Air Force Base, California. Captain Lacher was assigned to the School of Engineering, Air Force Institute of Technology, Wright-Patterson AFB, Ohio in May 1990.

Permanent address: 106 Ave San Luis Rey  
San Clemente, CA 92672

December 1991

Master's Thesis

AN EXPERIMENTAL STUDY OF A  
STING-MOUNTED CIRCULATION CONTROL WING

Steven J. Lacher, Captain, USAF

Air Force Institute of Technology  
WPAFB OH 45433-6583

AFIT/GAE/ENY/91D-4

Steven L. Williams  
ASD/XRH  
Wright-Patterson AFB OH 45433

Approved for public release; distribution  
unlimited

This wind tunnel study investigated the lift, drag, and pitching moment of a 20% thick, 8.5% camber, partial elliptical cross-section, single blowing slot, rectangular circulation control wing. The AFIT 5-foot wind tunnel was used. Lift and drag were referenced to the wind axis. The Reynolds number was  $5 \times 10^5$  for all tests. Angle of attack was varied from -6 to 16 degrees and the effects of pulsed blowing were investigated. Effects of tripping the Coanda jet with a small flow barrier attached spanwise along the Coanda surface were also studied. Results indicate that there is a limit on maximum lift obtainable by increasing circulation. The limit is presumed to be the result of three-dimensional effects. Pulsed blowing has little effect on average lift, but results in violent oscillation of the wing as the sting physically bends under cyclic loading. In certain situations, tripping the Coanda jet may reduce drag without decreasing lift.

134

Circulation Control, V/STOL Aircraft,  
Wind Tunnel Testing, Wing, Pulsed Blowing

Unclassified

Unclassified

Unclassified

UL